Molecular Pharmacology Fast Forward. Published on December 1, 2020 as DOI: 10.1124/molpharm.120.000169
This article has not been copyedited and formatted. The final version may differ from this version.

Predicting Drug Interactions with Human Equilibrative Nucleoside Transporters 1 and 2 Using Functional Knockout Cell Lines and Bayesian Modeling

Siennah R. Miller, Xiaohong Zhang, Raymond K. Hau, Joseph L. Jilek, Erin Q. Jennings, James J. Galligan, Daniel H. Foil, Kimberley M. Zorn, Sean Ekins, Stephen H. Wright & Nathan J. Cherrington

College of Pharmacy, Department of Pharmacology & Toxicology, University of Arizona, Tucson AZ, USA (SM, RH, JJ, EJ, JG, NC)

College of Medicine, Department of Physiology, University of Arizona, Tucson, AZ, USA (XZ, SW)

Collaborations Pharmaceuticals, Inc., Raleigh, NC, USA (DF, KZ, SE)

Downloaded from molpharm.aspetjournals.org at ASPET Journals on April 16, 2024

Molecular Pharmacology Fast Forward. Published on December 1, 2020 as DOI: 10.1124/molpharm.120.000169
This article has not been copyedited and formatted. The final version may differ from this version.

Running Title: Predicting Drug Interactions with ENT1 and ENT2

Corresponding Authors:

Nathan J. Cherrington

1295 N Martin Ave, Tucson, AZ, 85721

(520)-626-0219, cherring@pharmacy.arizona.edu

Stephen H. Wright

1501 N Campbell Ave, Tucson, AZ, 85724

(520)-626-4253, shwright@email.arizona.edu

Text Pages: **63**

Number of Tables: 4

Number of Figures: 11

Number of Supplemental Files: **2**

Number of References: 65

Number of Words in Abstract: 250

Number of Words in Introduction: 750

Number of Words in Discussion: 1499

Abbreviations:

BTB: Blood-Testis Barrier, MGT: Male Genital Tract, ENT: Equilibrative Nucleoside Transporter, NBMPR: S-[(4-nitrophenyl)methyl]-6-thioinosine, NRTI: Nucleoside Reverse Transcriptase Inhibitor, WB: Waymouth's Buffer, DDI: Drug-Drug Interaction, KO: Knockout, ROC: Receiver Operator Characteristic, LC-MS/MS: Liquid Chromatography Tandem Mass Spectrometry

Downloaded from molpharm.aspetjournals.org at ASPET Journals on April 16, 2024

Molecular Pharmacology Fast Forward. Published on December 1, 2020 as DOI: 10.1124/molpharm.120.000169
This article has not been copyedited and formatted. The final version may differ from this version.

Abstract

Equilibrative nucleoside transporters (ENT) 1 and 2 facilitate nucleoside transport across the blood-testis barrier (BTB). Improving drug entry into the testes with drugs that use endogenous transport pathways may lead to more effective treatments for diseases within the reproductive tract. In this study, CRISPR/Cas9 was used to generate HeLa cell lines in which ENT expression was limited to ENT1 or ENT2. We characterized uridine transport in these cell lines and generated Bayesian models to predict interactions with the ENTs. Quantification of [^{3}H]uridine uptake in the presence of the ENT specific inhibitor S-(4-nitrobenzyl)-6-thioinosine (NBMPR) demonstrated functional loss of each transporter. Nine nucleoside reverse transcriptase inhibitors and thirty-seven nucleoside/heterocycle analogs were evaluated to identify ENT interactions. Twenty-one compounds inhibited uridine uptake and abacavir, nevirapine, ticagrelor, and uridine triacetate had different IC_{50} values for ENT1 and ENT2. Total accumulation of four identified inhibitors was measured with and without NBMPR to determine if there was ENT-mediated transport. Clofarabine and cladribine were ENT1 and ENT2 substrates, while nevirapine and lexibulin were ENT1 and ENT2 non-transported inhibitors. Bayesian models generated using Assay Central® machine learning software yielded reasonably high internal validation performance (ROC > 0.7). ENT1 IC_{50}-based models were generated from ChEMBL; subvalidations using this training dataset correctly predicted 58% of inhibitors when analyzing activity by percent uptake and 63% when using estimated-IC_{50} values. Determining drug interactions with these transporters can be useful in identifying and predicting compounds that are ENT1 and ENT2

Downloaded from molpharm.aspetjournals.org at ASPET Journals on April 16, 2024

Molecular Pharmacology Fast Forward. Published on December 1, 2020 as DOI: 10.1124/molpharm.120.000169
This article has not been copyedited and formatted. The final version may differ from this version.

substrates, and can thereby circumvent the BTB through this transepithelial transport pathway in Sertoli cells.

Significance Statement

This study is the first to predict drug interactions with ENT1 and ENT2 using Bayesian modeling. Novel CRISPR/Cas9 functional knockouts of ENT1 and ENT2 in HeLa S3 cells were generated and characterized. Determining drug interactions with these transporters can be useful in identifying and predicting compounds that are ENT1 and ENT2 substrates, and can circumvent the blood-testis barrier through this transepithelial transport pathway in Sertoli cells.

Introduction

There is a need to understand and clarify the interactions between the equilibrative nucleoside transporters (ENTs) and nucleoside analogs. These ubiquitously expressed transporters play a role in the pharmacokinetics and drug-drug interactions (DDIs) of nucleoside analogs, which share a similar chemical structure to endogenous substrates of these transporters (Atlas, 2020; Huber-Ruano and Pastor-Anglada, 2009; Koczor et al., 2012; Pastor-Anglada and Pérez-Torras, 2015; Rehan et al., 2019). Although there is clear value in heterologous expression systems to study the ENTs, the resulting models can be complicated to interpret; the complexity owing to a variety of issues, including the influence of endogenous nucleoside transport activity (Boswell-Casteel and Hays, 2017; Sundaram, 2001; Ward et al., 2000; Yao et al., 2001). The disparity of published results using heterologous models highlights the value of experimental

Downloaded from molpharm.aspetjournals.org at ASPET Journals on April 16, 2024

Molecular Pharmacology Fast Forward. Published on December 1, 2020 as DOI: 10.1124/molpharm.120.000169
This article has not been copyedited and formatted. The final version may differ from this version.

systems with natively expressed ENTs, which have more consistent results in the literature (Boleti et al., 1997; Dahlig-Harley et al., 1981; Griffith and Jarvis, 1996; Lauzon G, 1977; Mackey et al., 1999; Miller et al., 2020; Plagemann et al., 1978; Ward et al., 2000). Recent work has pharmacologically separated native ENT1 and ENT2 activity in wild-type HeLa S3 cells with the ENT inhibitor 6-S-[(4-nitrophenyl)methyl]-6-thioinosine (NBMPR) (Miller et al., 2020) but there is need for a more efficient, high-throughput method of studying the interactions between individual ENTs and nucleoside analogs.

Nucleoside analogs are used to treat health conditions including viral infections and cancers by interfering with nucleic acid synthesis (Ewald et al., 2008; Jordheim et al., 2013). These include the nucleoside reverse transcriptase inhibitors (NRTIs), and DNA or RNA polymerase inhibitors used to treat various cancers, human immunodeficiency virus, and respiratory viruses (Ewald et al., 2008; Jordan et al., 2018; Jordheim et al., 2013; Lucas and Nelson, 2015). Nucleoside analogs have a long history of success and this class of therapeutics recently gained attention with the emergency use of the nucleotide analog remdesivir to treat COVID-19 (Eastman et al., 2020). Although there are many applications of nucleoside analogs, diseases that persist in sanctuary sites may be more difficult to treat because of the inability of compounds to reach effective concentrations. This includes the testis, where the blood-testis barrier (BTB) may prevent drugs from reaching therapeutically active concentrations within the male genital tract (MGT) (Durmus et al., 2015; Le Tortorec and Dejucq-Rainsford, 2010). The BTB protects developing germ cells from potentially harmful agents and can interfere

Downloaded from molpharm.aspetjournals.org at ASPET Journals on April 16, 2024

Molecular Pharmacology Fast Forward. Published on December 1, 2020 as DOI: 10.1124/molpharm.120.000169
This article has not been copyedited and formatted. The final version may differ from this version.

with drug disposition to the MGT (Miller and Cherrington, 2018; Mruk and Cheng, 2015). Some viruses are sexually transmitted and certain cancers negatively impact the structure and function of the MGT. SARS-CoV-2 viral loads are detectable in the semen of infected and recovering patients, indicating that it has the potential to be sexually transmitted (Cardona Maya et al., 2020; Li et al., 2020). Additionally, a clinical trial with Ebola virus survivors is investigating the potential of remdesivir to eradicate the virus from semen to prevent sexual transmission (National Institute of Allergy and Infectious Diseases, 2019). Therefore, it is essential that therapeutics reach effective concentrations in sanctuary sites to reduce viral transmission and/or eradicate the disease in question.

Transporters at the basal and apical membranes of testicular epithelial cells (Sertoli cells) provide a mechanism of bypassing the BTB (Miller and Cherrington, 2018; Mruk et al., 2011). ENT1 on the basal membrane and ENT2 on the apical membrane of Sertoli cells create a transepithelial transport pathway in which substrates of these transporters can enter the seminiferous lumen (Klein et al., 2013). Uridine is a well-established substrate of both ENT1 and ENT2 and can be used to study the interaction of various nucleoside analogs on its transport (Kato et al., 2005; Klein et al., 2013; Miller et al., 2020; Ward et al., 2000).

The present study generated the first CRISPR/Cas9 functional knockouts of ENT1 and ENT2 from HeLa S3 cells natively expressing both transporters; the ENT2-knockout cells retained functional ENT1 and the ENT1-knockout cells retained functional ENT2.

Downloaded from molpharm.aspetjournals.org at ASPET Journals on April 16, 2024

Molecular Pharmacology Fast Forward. Published on December 1, 2020 as DOI: 10.1124/molpharm.120.000169
This article has not been copyedited and formatted. The final version may differ from this version.

Interactions of endogenous nucleosides, nucleoside reverse transcriptase inhibitors (NRTIS), and an additional set of nucleoside/heterocycle analogs were studied to identify inhibitory interactions with ENT1 and ENT2. Additional transport studies were performed to determine if four identified inhibitors of the ENTs enter cells through an ENT-mediated mechanism. Bayesian machine learning was used to identify structural elements found in effective inhibitors of ENT1- and ENT2- mediated transport. Predicting interactions with these transporters can aid the development of novel compounds that can cross the BTB using the ENT1-ENT2 transepithelial transport pathway. These include novel antivirals and chemotherapeutics that are substrates for these widely expressed transporters.

Materials and Methods

Reagents

Oligonucleotide primers were purchased from Integrated DNA Technologies (Coralville, IA). Lysogeny broth (LB) and LB agar plates with 50 μg/mL ampicillin and LB were purchased through the University of Arizona BIO5 Media Facility. M-MLV reverse transcriptase, Platinum Taq DNA Polymerase High Fidelity, 10x BlueJuice gel loading buffer, UltraPure ethidium bromide and the Invitrogen Cells-to-cDNA II Kit were purchased from Invitrogen (Invitrogen, Carlsbad, CA). Phusion High-Fidelty PCR Mix with GC Buffer was purchased from New England Biolabs (Ipswich, MA). Quantum Prep Freeze ‘N Squeeze DNA Gel Extraction Spin Columns were purchased from BioRad (Hercules, CA). [^{3}H]Uridine (specific activity 35.2 Ci/mmol) was purchased from Perkin-Elmer (Waltham, MA). Uridine, adenosine, inosine, guanosine, cytidine, thymidine, and

Downloaded from molpharm.aspetjournals.org at ASPET Journals on April 16, 2024

Molecular Pharmacology Fast Forward. Published on December 1, 2020 as DOI: 10.1124/molpharm.120.000169
This article has not been copyedited and formatted. The final version may differ from this version.

nevirapine were purchased from Sigma-Aldrich (St. Louis, MO). 6-S-[(4-nitrophenyl)methyl]-6-thioinosine (NBMPR) was purchased from Tocris (Bristol, UK). Abacavir sulfate, entecavir hydrate, zidovudine, didanosine, lamivudine, emtricitabine, tenofovir disoproxil, stavudine, zalcitabine, clofarabine, cladribine, and lexibulin were purchased from Cayman Chemical (Ann Arbor, MI). Thirty-seven nucleoside/heterocycle analogs were identified from the literature, selected, and provided as a generous gift from Gilead Sciences Inc. (Foster City, CA). Additional reagents were purchased from Thermo-Fisher Scientific unless otherwise noted.

Cell Culture

HeLa S3 CCL-2.2 cells were purchased from ATCC™ and grown in Ham's F12K Media supplemented with 1.5 g/L sodium bicarbonate, 10% v/v fetal bovine serum, and 1% v/v penicillin and streptomycin as previously described (Miller et al., 2020). Cells were propagated using the ATCC™ protocol and kept at 37°C in a humidified 5% CO_2 incubator. Knockout HeLa S3 cell lines were cultured in the same conditions as wild-type HeLa S3 cells.

Generation of ENT1 and ENT2 HeLa Knockout Cell Lines

Guide RNA (gRNA) oligonucleotides for ENT1 and ENT2 were designed using the biology software Benchling (San Francisco, CA). The deletion for ENT1 was directed to be located in exon 5 with the gRNA forward sequence 5′-CACCGAGGTAGGTGAATAACAGCA -3' and the reverse sequence 5′-aaacTGCTGTTATTCACCTACCTC -3'. The deletion for ENT2 was directed to be

Downloaded from molpharm.aspetjournals.org at ASPET Journals on April 16, 2024

Molecular Pharmacology Fast Forward. Published on December 1, 2020 as DOI: 10.1124/molpharm.120.000169
This article has not been copyedited and formatted. The final version may differ from this version.

located in exon 1 with the gRNA forward sequence 5′-CACCGTGGCGCGAGGAGACGCCCCG -3’ and the reverse sequence 5’aaacCGGGGCGTCTCCTCGCGCCAC -3’. The pSp-Cas9(BB)-2A-GFP (PX458) plasmid, a gift from Feng Zhang (Addgene, Watertown, MA) (Ran et al., 2013), was prepared with gRNA inserts for either ENT1 or ENT2 as described by Cong et al. (Cong and Zhang, 2015). The PX458 plasmid containing the gRNA inserts for either ENT1 or ENT2 was transformed into DH5α cells (New England Biolabs, Ipswich, MA). The transformed DH5α cells were then inoculated on LB agar plates containing 50 μg/mL ampicillin and incubated at 37°C overnight. Single colonies were then inoculated into LB supplemented with 100 μg/mL ampicillin and incubated at 37°C overnight in a shaker at 250 RPM. A QIAprep Spin Miniprep Kit (Qiagen, Hilden, Germany) was used to purify the plasmid DNA according to the manufacturer’s protocol. Concentration of the plasmid DNA was determined using a Spectrophotometer NanoDrop ND-1000 (ThermoFisher Scientific, Waltham, MA). The purified plasmids were sequenced with the primer: 5’-TTTATGGCGAGGCGGCG -3’ to confirm successful integration of the gRNA inserts.

Wild-type HeLa S3 cells were seeded 200,000 cells/well in a six-well plate one day prior to transfection. Cells were incubated with a mixture of 5 μL of Lipofectamine 3000, 1.25 μL of P3000, 1.2 μg of plasmid DNA with gRNA inserts for ENT1 or ENT2 in 2 mL of Opti-MEM per well for 24 hours at 37°C. Media was replaced 24 hours later and cells were allowed to recover for 24 hours. Cells were passed and collected in preparation for fluorescence-assisted single cell sorting using the BD FACSAria III at the Cytometry Core Facility at the University of Arizona. Data was analyzed using BD FACSDiva

Downloaded from molpharm.aspetjournals.org at ASPET Journals on April 16, 2024

Molecular Pharmacology Fast Forward. Published on December 1, 2020 as DOI: 10.1124/molpharm.120.000169
This article has not been copyedited and formatted. The final version may differ from this version.

version 8.0.2. Single fluorescing cells were sorted into individual wells of two 96-well plates per cell line. Clones were maintained until a sufficient number of cells were obtained to assess successful knockout of either ENT1 or ENT2 (Cong and Zhang, 2015; Gaffney et al., 2019).

Polymerase Chain Reaction and Sanger Sequencing

The Invitrogen Cells-to-cDNA II Kit was used to generate cDNA from wild-type HeLa S3 cells, ENT1 KO cells, and ENT2 KO cells. Approximately 100,000 cells per cell line were harvested and prepared for reverse transcription. Briefly, 10 μL of the lysate was incubated with 1 μL of 10 mM dNTPs and 1 μL of Oligio$(dT)_{18}$ primers at 65°C for 5 minutes and briefly chilled on ice. Next, 4 μL of 5x first strand buffer, 2 μL of 0.1 mM DTT, 1 μL of M-MLV reverse transcriptase and 1 μL of RNAse inhibitor were added (final volume 20 μL) and incubated at 37°C for 50 minutes and then 70°C for 15 minutes.

For PCR amplification of ENT1, 3.5 μL of the cDNA, 1 μL of 10 mM dNTPs, 0.3 μL Platinum Taq DNA Polymerase High Fidelity, 5 μL of 10X PCR buffer, 1.5 μL of 50 mM $MgSO_4$, 36.7 μL of H_2O and 1 μL each of 10 μM forward and reverse primers (total volume of 50 μL) were incubated at 94°C for 3 minutes followed by 35 cycles of: 94°C 45 seconds, 54°C for 30 seconds and 72°C for 1 minute. Following the 35 cycles, the reaction was incubated at 72°C for 10 minutes for final extension. The primers amplify the region containing the deletion. For ENT1, the product size was 419 base pairs with a forward sequence of 5′- GAGGCTGGAGGGACTGGGCTCC -3′ and a reverse

Downloaded from molpharm.aspetjournals.org at ASPET Journals on April 16, 2024

Molecular Pharmacology Fast Forward. Published on December 1, 2020 as DOI: 10.1124/molpharm.120.000169
This article has not been copyedited and formatted. The final version may differ from this version.

sequence of 5′- CAAGGGTGGCAGAGACAAGTGG -3’. Different reaction conditions and PCR buffer were necessary to amplify ENT2 due to high GC content. Briefly, 5 μL of forward and reverse primers (10 μM each), 1.5 μL DMSO, 25 μL 2x NEB Phusion High-Fidelity PCR Master Mix with GC Buffer, 3 μL of cDNA and 15.5 μL of H_2O were incubated at 98°C for 30 seconds, followed by 35 cycles of 98°C for 10 seconds, 68°C for 30 seconds and 72°C for 30 seconds, and a final extension of 10 minutes at 72°C. The product size was 794 base pairs with a forward sequence of 5′-GTGGGTTCCAGCTTTAGGGGTC-3′ and a reverse sequence of 5′-GGGATCGGTGGGAAGGTCACCC -3’.

BlueJuice 10x gel loading buffer (Invitrogen, Carlsbad, CA) was added to the PCR product and 45 μL was loaded onto a 1% w/v agarose gel containing ethidium bromide and run for approximately 25 minutes at 130 V. PCR product was visualized using ultraviolet light and bands corresponding to correct product sizes were excised and immediately extracted using Quantum Prep Freeze ‘N Squeeze Gel Extraction Spin Columns (Bio-Rad, Hercules, CA). Samples were submitted for Sanger sequencing at the University of Arizona Genetics Core.

Real-Time qPCR

cDNA was generated as described above and diluted 1:25 before real-time qPCR. Each reaction contained 2 μL of diluted cDNA, 5 μL of PerfeCTa SYBR Green FastMix (Quantabio, Beverly, MA), 1 μL each of 1 μM forward and reverse primers, and 1 μL of H_2O. Each reaction was performed in duplicate per passage, with three passages for

Downloaded from molpharm.aspetjournals.org at ASPET Journals on April 16, 2024

Molecular Pharmacology Fast Forward. Published on December 1, 2020 as DOI: 10.1124/molpharm.120.000169
This article has not been copyedited and formatted. The final version may differ from this version.

each cell line. The reaction conditions were: 95°C for 5 minutes, followed by 45 cycles of 95°C for 15 seconds and 60°C for 30 seconds using the Rotor-Gene RG-3000 (Corbett Research, San Francisco, CA). Specific primers for ENT1, ENT2 and GAPDH were designed using Primer3 software (Rozen and Skaletsky, 2000) to the 3' end of the genes and primers were synthesized by Integrated DNA Technologies (Coralville, IA). The primers for ENT1 are located in exon 14 with a product size of 131 base pairs with a forward sequence of 5′-GCTGGGTCTGACCGTTGTAT-3′ and a reverse sequence of 5′-CTGTACAGGGTGCATGATGG -3'. The primers for ENT2 are located in exon 12 with a product size of 164 base pairs and a forward sequence of 5′-AGCCTGCATGTGTGTACTGC-3′ and a reverse sequence of 5′-ACCACGGACCAGTCACTTTC -3′. The primers for GAPDH were: forward sequence of 5′-CGACCACTTTGTCAAGCTCA-3′ and a reverse sequence of 5′-CCCTGTTGCTGTAGCCAAAT-3′. Cycle threshold values (C_t) values relative to GAPDH expression levels in respective samples were used to determine expression levels of ENT1 and ENT2 using the $2^{-\Delta\Delta Ct}$ method (Livak and Schmittgen, 2001). Expression data is presented as mean fold change (± S.D).

Cell Growth

Growth rate was assessed for wild-type HeLa S3 cells, ENT1 KO (ENT2) and ENT2 KO (ENT1) cells. Cells were seeded at 30,000 cells/well in 6-well plates, with duplicate wells per day of cell counting. Cells were counted daily using the Nexcelom Bioscience Cellometer Auto T4 cell counter for five days and media was changed every other day. Doubling time was calculated from average cell count from two separate experiments.

Downloaded from molpharm.aspetjournals.org at ASPET Journals on April 16, 2024

Molecular Pharmacology Fast Forward. Published on December 1, 2020 as DOI: 10.1124/molpharm.120.000169
This article has not been copyedited and formatted. The final version may differ from this version.

Transport Experiments

Transport experiments were performed as previously described (Miller et al., 2020). All transport buffers were made with Waymouth's Buffer (WB; 2.5 mM $CaCl•2H_2O$, 28 mM D-glucose, 13 mM HEPES, 135 mM NaCl, 1.2 mM $MgCl_2$, 0.8 mM $MgSO_4•7H_2O$, pH 7.4), 1 μCi/mL (approximately 20 nM) [^{3}H]uridine and selected test compounds. Test compound and transport buffer containing [^{3}H]uridine was added to cells simultaneously, with no pre-incubation of test compounds on cells. Inhibition of [^{3}H]uridine uptake by NRTIs was tested at 100 μM, 300 μM and 1 mM (Supplemental Table 1, Figure 6). All compounds from Gilead Sciences Inc. arrived as 10 mM solutions in DMSO (Supplementary Table 2). 200 μM of each compound was used for experiments to maximize the concentration of the compound used and to remain below 2% final DMSO (v/v). All controls (100 nM and 100 μM NBMPR, 200 μM adenosine, guanosine, thymidine, inosine, and cytidine) contained 2% DMSO (v/v). Cells (200,000 cells/mL) were seeded into separate Nunc MicroWell 96-well optical bottom plates (ThermoFisher Scientific, Waltham, MA) for next day experiments. Media was aspirated and cells were washed once with 300 μL of room temperature WB using a Biotek 405 LS Microplate Washer (BioTek, Winooski, VT) before initiating transport by adding 50 μL of transport buffer containing compounds of interest and [^{3}H]uridine using an Integra VIAFLO 96-well multichannel pipette (Integra Lifesciences, Plainsboro, NJ). Transport was terminated after two or seven minutes as indicated in the figure legends by rinsing twice with WB. After washing, 200 μL of MicroScint-20 scintillation cocktail (Perkin-Elmer, Waltham, MA) was added to each well before sealing with microplate film and incubating at room temperature in the dark for at least two hours. Total accumulated

Downloaded from molpharm.aspetjournals.org at ASPET Journals on April 16, 2024

Molecular Pharmacology Fast Forward. Published on December 1, 2020 as DOI: 10.1124/molpharm.120.000169
This article has not been copyedited and formatted. The final version may differ from this version.

radioactivity was determined with a Wallac 1450 MicroBeta TriLux liquid scintillation counter (Perkin-Elmer, Waltham, MA).

Determination of Transport by LC-MS/MS

Transport experiments for LC-MS/MS were completed as described above using 50 μM of lexibulin, clofarabine, and cladribine for both cell lines, 50 μM of nevirapine for ENT2 cells and 100 μM nevirapine for ENT1 cells. Uptake of compounds was measured in the presence or absence of 100 μM NBMPR. Preliminary experiments determined that an incubation time of 5 minutes produced a detectable transport signal for these compounds, therefore, transport was terminated after 5 minutes. Samples were prepared as described in (Miller et al., 2020). Briefly, after terminating transport, 50 μL of 1:1 methanol:ACN was added to cells containing 10 ng/mL of internal standard and incubated overnight at 4°C. The internal standard was abacavir for lexibulin and nevirapine. The internal standard for clofarabine was cladribine, and vice versa. Calibration curves were also prepared in methanol:ACN and treated identically to samples. Samples were dried and resuspended in 50 μL of 90:10 H_2O:ACN + 0.1% formic acid for lexibulin and nevirapine, and in 50 μL of H_2O + 0.1% formic acid for clofarabine and cladribine. Debris was removed by centrifuging at maximum speed for 10 minutes in a table-top centrifuge and the supernatant was collected for LC-MS/MS analysis.

A Shimadzu Prominence HPLC system (Shimadzu, Kyoto, Japan) coupled to a SCIEX QTRAP 4500 mass spectrometer (SCIEX, Framingham, MA) was used to detect

Downloaded from molpharm.aspetjournals.org at ASPET Journals on April 16, 2024

Molecular Pharmacology Fast Forward. Published on December 1, 2020 as DOI: 10.1124/molpharm.120.000169
This article has not been copyedited and formatted. The final version may differ from this version.

intracellular accumulation of selected compounds. Clofarabine, cladribine, nevirapine, lexibulin and abacavir were detected by positive electrospray ionization with the following source parameters: 5.5 kV ion spray voltage, 500 ℃ source temperature, 20 psi nebulizer gas, 40 psi turbo gas, and 9 psi collision gas. Analyte intensity was determined by multiple reaction monitoring (MRM) as noted in Supplementary Table 3. 10 μL of each sample was injected onto a Luna Omega polar C18 column (50 x 2.1 mm with 1.6 μm bead diameter; Phenomenex, Torrance, CA). For clofarabine and cladribine, analytes were separated over a binary gradient consisting of H_2O with 0.1% formic acid (A) and acetonitrile with 0.1% formic acid (B) at a flow rate of 0.3 mL/min as follows: 0% B (0-1 min), 0 to 80% B (1-5 min), hold at 80% B for one minute, followed by a decrease from 80 to 0% B (6-7.5 min). Lexibulin, nevirapine and abacavir analytes were separated over a binary gradient consisting of water with 0.1% formic acid (A) and acetonitrile with 0.1% formic acid (B) at a flow rate of 0.3 mL/min as follows: 10 % B (0-1 min), 10 to 90% B (1-3 min), 90% B (3-4 min), 90 to 10% B (4-4.5 min), and 10% B (4.5-6 min).

Assay Central® Bayesian Models

Assay Central® software was used to build machine learning models and prediction generation methods, and evaluate metrics of predictive performance and the interpretation of prediction and applicability scores as previously described (Clark et al., 2015; Clark and Ekins, 2015, Zorn et al., 2019). Initially, a series of scripts employing standardized rules were applied to detect problematic data (including abnormal valences and mixtures) and correct it by multiple methods (i.e. structures were desalted

Downloaded from molpharm.aspetjournals.org at ASPET Journals on April 16, 2024

Molecular Pharmacology Fast Forward. Published on December 1, 2020 as DOI: 10.1124/molpharm.120.000169
This article has not been copyedited and formatted. The final version may differ from this version.

and neutralized, finite activities merged, potentially incorrect structures are flagged for review) to then output a high-quality structure-activity dataset. A Bayesian algorithm is then applied to the structure-activity datasets generating extended-connectivity fingerprints (ECFP6) as molecular descriptors for structures, and the corresponding activity is either binary or set according to a user-defined threshold for a Boolean classification (Clark et al., 2015; Clark and Ekins, 2015). The resulting machine learning model can be used to predict the probability of target activity from chemical structure alone. Prospective molecule applicability was evaluated by a score in which a higher value suggested higher fragment representation in the model to ensure a given prediction is within the scope of the training data. Prediction scores were evaluated according to the standard probability cutoff, where a value of ≥ 0.5 designates a chemical as active (Clark et al., 2015; Clark and Ekins, 2015).

Herein, we have applied Assay Central® machine learning methods to ENT1 and ENT2 inhibition of [^{3}H]uridine uptake into cells. Bayesian machine learning models were constructed from the percent uptake data generated from 44 unique compounds: 37 compounds provided in Supplemental Table 2 and five endogenous nucleosides, as well as three tracers (two unique). Training data was binarized so that an active compound (i.e. an inhibitor of ENT1 or ENT2) was considered one which inhibited >50% average [^{3}H]uridine uptake. No structural corrections were necessary.

Additionally, we externally validated a machine learning model built from ChEMBL IC_{50} data to evaluate if machine learning could correctly predict the ENT1 results generated

Downloaded from molpharm.aspetjournals.org at ASPET Journals on April 16, 2024

Molecular Pharmacology Fast Forward. Published on December 1, 2020 as DOI: 10.1124/molpharm.120.000169
This article has not been copyedited and formatted. The final version may differ from this version.

in this study. Specifically, training data was pulled from Target ID 1997 (https://www.ebi.ac.uk/chembl/target_report_card/CHEMBL1997/) for human ENT1, and the activity threshold was set so that a compound was considered active if the reported IC_{50} was < 100 μM. The two test sets were comprised of all compounds (Supplemental Table 2), five endogenous nucleosides and three additional compounds); all compounds had percent uptake and 27 had estimated-IC_{50} data against ENT1. Estimated-IC_{50} values were calculated using Equation 4 and uptakes determined in the absence of inhibitor and in the presence of each inhibitor at 200 μM. Five compounds were in the training model ([^{3}H]uridine + 5 mM uridine, [^{3}H]uridine +100 nM NBMPR, [^{3}H]uridine +100 μM NBMPR adenosine, and tecadenoson) and they were removed from this test set. Testing compounds were binarized so that an active compound was considered one that produced <50 % of control uptake or an estimated-IC_{50} < 100 μM. External validation, which we term a “subvalidation”, was applied within Assay Central® so that the binarized ChEMBL training set was applied to predict each individual test set and output performance metrics. Individual predictions that culminate in these metrics are provided in Supplemental File 1 with the five removed compounds noted as “In model” for the applicability score. Only minimal structural corrections were necessary (i.e. removing salt components, omitting 49 compounds that did not provide an IC_{50} value). Additional information on the generation of Assay Central® Bayesian Models is included in the supplemental files under “Assay Central® User Manual” of Sandoval et. al., 2018.

Data Analysis

Downloaded from molpharm.aspetjournals.org at ASPET Journals on April 16, 2024

Molecular Pharmacology Fast Forward. Published on December 1, 2020 as DOI: 10.1124/molpharm.120.000169
This article has not been copyedited and formatted. The final version may differ from this version.

Each experiment was completed with cells cultured from multiple passages and multiple replicates per passage as indicated in the figure legends and predetermined before conducting the experiment. Data is presented as mean ± standard deviation (S.D) unless otherwise noted, and completed using GraphPad Prism 8 (San Diego, CA). For analysis of cell growth data, two-way analysis of variance (ANOVA) with Sidak's correction for multiple comparisons (12 comparisons per family) was used to compare the mean cell count of knockout cells to wild-type cells ($p<0.05$). Doubling time was calculated by fitting the exponential growth equation to cell growth data

Equation 1: $Doubling\ time = Y_0 e^{k*X}$

Where Y_0 is the initial amount of cells seeded (30,000), X is hours, and k is the rate constant.

The IC_{50} value of NBMPR, abacavir, nevirapine, lexibulin, clofarabine, and cladribine on ENT1- and ENT2- mediated [^{3}H]uridine uptake, was determined using the following equation:

Equation 2:

$$J = \frac{J_{app} * [T]}{IC_{50} + [S]} + K_d * [T]$$

Downloaded from molpharm.aspetjournals.org at ASPET Journals on April 16, 2024

Molecular Pharmacology Fast Forward. Published on December 1, 2020 as DOI: 10.1124/molpharm.120.000169
This article has not been copyedited and formatted. The final version may differ from this version.

Where J is total uridine transport J_{app} is a constant (J_{max} for uridine times the ratio of the IC_{50} for the inhibitor and the K_t for uridine), T is [^{3}H]uridine concentration, S is NBMPR concentration. We estimated the initial rate of uridine uptake at two minutes. The non-saturable/mediated component of total net accumulation, K_d, was determined using Equation 3a and has units of μL•cm^{-2}•min^{-1}. This value was subtracted from total uridine uptake at each substrate concentration to generate values for J_{max} and K_t (Equation 3b), as previously described for wild-type HeLa cells (Miller et al., 2020):

Equation 3a:

$$J = \frac{J_{max} * [S]}{K_t + [S]} + K_d * [S]$$

Equation 3b:

$$J = \frac{J_{max} * [S]}{K_t + [S]}$$

An unpaired two-tailed t-test was used to calculate the statistical difference between each kinetic parameter, NBMPR IC_{50} values, and transport determination studies ($p<0.05$ indicating a difference in kinetic parameters or NBMPR IC_{50} values, $p>0.05$ indicating no difference). An extra-sum of squares F-test and comparison of fits was used to calculate the statistical difference between IC_{50} values generated from best-fit lines for endogenous nucleosides and estimated-IC_{50} values for nucleoside analog/heterocycle analog interaction studies ($p<0.05$ indicating an difference in IC_{50} values between ENT1 and ENT2, $p>0.05$ indicating no difference). Data in Table 2-4 are presented as mean and 95% confidence intervals. Ordinary one-way ANOVA with

Downloaded from molpharm.aspetjournals.org at ASPET Journals on April 16, 2024

Molecular Pharmacology Fast Forward. Published on December 1, 2020 as DOI: 10.1124/molpharm.120.000169
This article has not been copyedited and formatted. The final version may differ from this version.

Dunnett's correction for multiple comparisons, comparing the mean of a column to the control column (i.e. [^{3}H]uridine uptake only), was used for experiments with NRTIs (Figure 6) and nucleoside/heterocycle analogs (Figure 7). For nucleoside/heterocycle analogs that inhibited [^{3}H]uridine uptake, a comparison of fits of Equation 4 and extra sum-of-squares F-test was done to compare the values for each cell line. IC_{50} values for these compounds were estimated from inhibition experiments using Equation 4 as previously described (Kido et al., 2011; Sandoval et al., 2018):

Equation 4:

$$J = \frac{J_0}{1 + \frac{I}{Estimated\ IC_{50}}}$$

Where J_0 represents ENT-mediated transport rate in the absence of the inhibitor and J represents ENT-mediated transport rate in the presence of the inhibitor. I is the inhibitor concentration (200 μM).

Results

Generation and Characterization of ENT1 and ENT2 Knockout Cell Lines

Successful deletion of ENT1 and ENT2 was confirmed in HeLa S3 cells using PCR and Sanger sequencing. Figure 1A and B show the location of the deletions in each cell line. For the ENT1 KO cells, there is a two nucleotide deletion in exon 5. For the ENT2 KO cells, there is a fourteen nucleotide deletion in exon 1. Hereafter, these cell lines are referred to as ENT1 or ENT2 cells, named after the transporter that remains functional. Cell growth of the newly generated cell lines was also assessed. After five days in

Downloaded from molpharm.aspetjournals.org at ASPET Journals on April 16, 2024

Molecular Pharmacology Fast Forward. Published on December 1, 2020 as DOI: 10.1124/molpharm.120.000169
This article has not been copyedited and formatted. The final version may differ from this version.

culture, both cell lines had a lower total cell count than wild-type HeLa S3 cells (Figure 1C) ($p<0.001$ for ENT1 cells, $p<0.05$ for ENT2 cells). The doubling time was calculated using equation 1. For wild-type HeLa cells, the doubling time was 22.78 hours (95% CI: 18.47, 27.95). For ENT1 cells, the doubling time was 22.0 hours (95% CI: 17.55, 27.41) For ENT2 cells, the doubling time was 22.14 hours (95% CI: 18.43, 26.48). The mRNA expression levels were measured in both knockout cell lines relative to wild-type HeLa cells (Figure 1D). The mRNA expression of ENT1 and ENT2 modestly decreased relative to wild-type cells in the ENT1 cells. However, in ENT2 cells, mRNA expression of both ENT1 and ENT2 decreased relative to wild-type cells.

Functional Assessment of ENT1 and ENT2 Cell Lines

We measured the accumulation of [^{3}H]uridine over the course of seven minutes in both cell lines in order to evaluate the functional loss of ENT1 or ENT2. A saturating concentration of unlabeled uridine (5 mM) was used to establish the fraction of total uridine accumulation that was carrier-mediated. Although there was only a modest decrease in mRNA expression of ENT2, >96% of [^{3}H]uridine uptake was mediated by ENT1 in ENT1 cells (Figure 2A). In ENT2 cells, >90% of [^{3}H]uridine uptake was mediated by ENT2 (Figure 2B). The IC_{50} of NBMPR for each transporter was determined using Equation 2. For ENT1, the IC_{50} was 13.81 (95% CI: -0.104, 28.66) nM and for ENT2, the IC_{50} was 1.85 (95% CI: 0.245, 3.44) μM (Figure 3, $p=0.0078$).

Kinetics of Uridine Transport

Downloaded from molpharm.aspetjournals.org at ASPET Journals on April 16, 2024

Molecular Pharmacology Fast Forward. Published on December 1, 2020 as DOI: 10.1124/molpharm.120.000169
This article has not been copyedited and formatted. The final version may differ from this version.

[^{3}H]Uridine uptake was effectively linear for seven minutes in wild-type HeLa cells and in the ENT1 and ENT2 cells (Miller et al., 2020). To determine uridine transport kinetics in each cell line, we evaluated [^{3}H]uridine uptake after two minutes to estimate the initial rate of uptake. The J_{max} for ENT1 was 23.8 ± 0.9 pmol•cm^{-2}•min^{-1} and for ENT2 was 44.9 ± 16.3 pmol•cm^{-2}•min^{-1} (p=0.089). The K_t for ENT1 was 13.8-fold lower than for ENT2 (11.4 ± 3.9 and 156.9 ± 55.6 μM, p=0.016) (Figure 4, Table 1). The ratios of the kinetic parameters are also presented in Table 1.

Endogenous Nucleoside Interactions

We examined the differences in inhibition of [^{3}H]uridine uptake in the ENT1 and ENT2 cell lines determined in the presence of the endogenous nucleosides: adenosine, guanosine, thymidine, inosine and cytidine (Figure 5, Table 2). A best-fit line was generated from Equation 2 to generate IC_{50} values and an extra-sum of squares F-test ($p<0.05$ indicating a statistical difference in IC_{50} values, $p>0.05$ indicating no statistical difference in IC_{50} values) was used for comparison. For adenosine, the IC_{50} was 39.9 (95% CI: 24.5, 65.14) μM for ENT1 and 56.5 (95% CI: 29.3, 108.5) μM for ENT2 (p=0.3767). For guanosine, the IC_{50} for ENT1 was 385.9 (95% CI: 194.4, 780.5) μM and 254.9 (95% CI: 140.5, 458.6) μM for ENT2 (p=0.3582). The IC_{50} value for thymidine was 5.1-fold lower for ENT2 than ENT1 138.1 (95% CI: 64.7, 290.4) μM and 708.9 (95% CI: 368.6, 1468.0) μM, p=0.0014). The IC_{50} for inosine was 8.1-fold lower for ENT2 than ENT1 (27.0 (95% CI: 19.5, 37.5) μM and 219.5 (95% CI: 113.1, 426.4) μM, $p<0.0001$). The IC_{50} for cytidine was 17.5-fold lower for ENT1 than ENT2 (21.1 (95% CI: 12.2, 36.7)

Downloaded from molpharm.aspetjournals.org at ASPET Journals on April 16, 2024

Molecular Pharmacology Fast Forward. Published on December 1, 2020 as DOI: 10.1124/molpharm.120.000169
This article has not been copyedited and formatted. The final version may differ from this version.

μM and 368.2 (95% CI: 105.3, 1338.0) μM, p<0.0001). The ratios of the IC_{50} values for ENT2 and ENT1 are shown in Table 2.

NRTI Interactions

Nine NRTIs (abacavir, zidovudine, entecavir, zalcitabine, lamivudine, emtricitabine, didanosine, stavudine and tenofovir disoproxil) (Figure 6, Supplemental Table 1) were evaluated for their impact on [^{3}H]uridine uptake. The selected NRTIs have molecular weights below 300 g/mol except tenofovir disoproxil. These NRTIs were tested at 100 μM, 300 μM and 1 mM in Figure 6 as previously described (Miller et al., 2020). Only abacavir inhibited [^{3}H]uridine uptake at all three concentrations for both cell lines. Zidovudine inhibited uptake at 300 μM and 1 mM in both cell lines. Entecavir inhibited [^{3}H]uridine uptake at 1 mM in ENT2 cells. Emtricitabine modestly inhibited uptake at all concentrations in ENT2 cells. Since abacavir was the most potent inhibitor of the nine NRTIs tested, we determined its IC_{50} for ENT1 and ENT2 (Figure 8A). There IC_{50} values of abacavir were 85.7 (95% CI: 34.2, 137.3) μM for ENT1 and 316.8 (95% CI: 113.3, 520.2) μM for ENT2 (p=0.0056).

Nucleoside/Heterocycle Analog Interactions

Thirty-seven nucleoside/heterocycle analogs (Supplemental Table 2) were tested at 200 μM to evaluate their impact on [^{3}H]uridine uptake (Figure 7). This concentration was used to maximize the concentration of the compound used while still remaining below 2% DMSO (v/v) to prevent interference with transport. Seventeen compounds inhibited uptake in at least one cell line. For ENT1, estimated-IC_{50} values ranged from 4-209 μM

Downloaded from molpharm.aspetjournals.org at ASPET Journals on April 16, 2024

Molecular Pharmacology Fast Forward. Published on December 1, 2020 as DOI: 10.1124/molpharm.120.000169
This article has not been copyedited and formatted. The final version may differ from this version.

and for ENT2, estimated-IC_{50} values ranged from 23-441 μM. Nevirapine, ticagrelor and uridine triacetate had different estimated-IC_{50} values for ENT1 and ENT2 (p=0.0026, p=0.0007 and p=0.0013, respectively, Table 3). The ratios of the estimated-IC_{50} values for ENT2 and ENT1 are shown in Table 3. Using this method to estimate IC_{50} values, thymidine, inosine, and cytidine had differing values for ENT1 and ENT2 (p=0.0152, p=0.014, p=0.0001, respectively) that reflected the results from full IC_{50} curves in Figure 5. Full IC_{50} values were determined for nevirapine, lexibulin, clofarabine and cladribine using Equation 2 (Figure 8B-E). Nevirapine inhibited 50% of [^{3}H]uridine uptake for ENT1 at 166.8 μM (95% CI: -32.88, 366.6) and 17.78 μM (95% CI: 2.83, 32.73) for ENT2 (p=0.011). Lexibulin inhibited 50% of [^{3}H]uridine uptake for ENT1 at 16.49 μM (95% CI: 0.776, 32.20) and 21.32 μM (95% CI: -2.24, 44.89) for ENT2 (p=0.722). Clofarabine inhibited 50% of [^{3}H]uridine uptake for ENT1 at 31.48 μM (95% CI: 11.83, 51.13) and 12.22 μM (95% CI: 2.53, 21.91) for ENT2 (p=0.051). Cladribine inhibited 50% of [^{3}H]uridine uptake for ENT1 at 67.26 μM (95% CI: 28.10, 106.40) and 40.15 μM (95% CI: 15.06, 65.24) for ENT2 (p=0.170).

Transport Determination for Nevirapine, Lexibulin, Clofarabine and Cladribine

Accumulation of clofarabine, cladribine, nevirapine and lexibulin was measured in the absence and presence of NBMPR and detected by LC-MS/MS (Figure 9). A decrease in clofarabine uptake was detected in the presence of NBMPR in ENT1 and ENT2 cells (p=0.026, p=0.0482). Similarly, a decrease in cladribine uptake was detected in the presence of NBMPR in ENT1 and ENT2 cells (p=0.0031, p=0.0096). No change in

Downloaded from molpharm.aspetjournals.org at ASPET Journals on April 16, 2024

Molecular Pharmacology Fast Forward. Published on December 1, 2020 as DOI: 10.1124/molpharm.120.000169
This article has not been copyedited and formatted. The final version may differ from this version.

nevirapine uptake in the presence of NBMPR was detected in ENT1 or ENT2 cells (p=0.1502, p=0.9691). No change in lexibulin uptake was observed in the presence of NBMPR in ENT1 cells (p=0.1589), but an increase in uptake was detected in the presence of NBMPR in ENT2 cells (p=0.0340).

Assay Central® Bayesian Models

Bayesian models were generated for ENT1 and ENT2 using percent uptake of control (i.e. [^{3}H]uridine uptake only) in the presence of 37 nucleoside analogs (200 μM), 5 mM uridine, 100 μM NBMPR, and five endogenous nucleosides (200 μM), for a total of 44 compounds in each model. Inhibitors were classified as “active” if uptake was reduced by at least 50%; there were 18 active compounds for ENT1 and 17 active compounds for ENT2. Both the ENT1 and ENT2 models (Figure 10) performed similarly and produced high performance metrics. Receiver operator characteristic (ROC) scores exceeded 0.71, with recall and specificity metrics ranged from 0.69-0.77. For small datasets, these scores are acceptable. The truth tables below the ROC curves indicate the number compounds that were of true positive (predicted and are inhibitors), false positive (type 1 error; predicted to be inhibitors and were not), true negative (were not predicted and are not inhibitors) and false negative (type 2 error; were not predicted and were inhibitors). Additional statistics presented in Figures 10 and 11 include (i) precision, (ii) recall (sensitivity, i.e., true positive rate), (iii) specificity (i.e. true negative rate), (iv) F1 score, (v) Kappa, and (vi) MCC (i.e. overall model classification performance). Equations and descriptions for these parameters for model statistics are previously described (Carletta, 1996; Cohen, 1960; Matthews, 1975; Zorn et al., 2019).

Downloaded from molpharm.aspetjournals.org at ASPET Journals on April 16, 2024

Molecular Pharmacology Fast Forward. Published on December 1, 2020 as DOI: 10.1124/molpharm.120.000169
This article has not been copyedited and formatted. The final version may differ from this version.

These common metrics for evaluating machine learning model performance indicate that future prospective predictions can be reasonably considered, as the internal predictive performance is better than random chance.

External validation, or Assay Central® subvalidations, were also performed for ENT1, where test set compounds were classified as inhibitors if the prediction thresholds were above 0.5. The ENT1 training model was built from all IC_{50} data available from ChEMBL Target ID 1997, and the threshold was set at 100 µM (Figure 11A). The estimated-IC_{50} values were calculated from the rates of transport measured in the absence of inhibitor and in the presence of 200 µM concentrations of a battery of test inhibitors) compounds ([I]), i.e., J_0 and J_i, respectively, using the equation 4 (Kido et al., 2011; Sandoval et al., 2018). These calculated values are referred to as 'estimated' IC_{50} values. The test set was composed of the 37 nucleoside/heterocycle analogs, endogenous nucleosides, and NBMPR and uridine, with percent uptake and estimated-IC_{50} data generated using Equation 4 using two points: [^{3}H]uridine and 200 M of compound. Five compounds were in the training model (adenosine, [^{3}H]uridine + 5 mM uridine, [^{3}H]uridine + 100 nM NBMPR, [^{3}H]uridine + 100 µM NBMPR, and tecadenoson), so they were removed from the test set. The individual predictions summarized in the truth table for each transporter test set have also been made available (Supplemental File 1). The first test set for ENT1 subvalidation (Figure 11B) was defined by binary classification of percentage uptake less than 50%, totaling 40 compounds. The public training dataset correctly predicted 58% of inhibitors. The second test set for ENT1 subvalidation (Figure 11C) was defined by binary classification of estimated-IC_{50} values of less than 100 µM with

Downloaded from molpharm.aspetjournals.org at ASPET Journals on April 16, 2024

Molecular Pharmacology Fast Forward. Published on December 1, 2020 as DOI: 10.1124/molpharm.120.000169
This article has not been copyedited and formatted. The final version may differ from this version.

27 compounds total. In this case the public training dataset correctly predicted 63% of test set inhibitors.

Discussion

This study generated CRISPR/Cas9 functional knockouts of ENT1 and ENT2 in HeLa S3 cells with deletions in exon 5 and exon 1, respectively (Figure 1A). In ENT1 cells, > 96% of [^{3}H]uridine uptake was mediated by ENT1 (Figure 2A). In ENT2 cells 90% of [^{3}H]uridine uptake was mediated by ENT2 (Figure 2B). The ENT1 cells showed approximately 2.4 times the ENT1-mediated [^{3}H]uridine uptake observed in wild-type HeLa S3 cells when ENT activity was pharmacologically separated using NBMPR, and 1.8 times the amount of total combined ENT1 and ENT2 mediated- [^{3}H]uridine uptake (Miller et al., 2020). The ENT2 cells showed approximately 1.4 times the observed ENT2-mediated [^{3}H]uridine uptake in wild-type HeLa S3 cells (Miller et al., 2020). There were no differences in the growth rate of wild-type and ENT cells (Figure 1C). We saw decreases in ENT1 and ENT2 mRNA expression for ENT2 cells, and modest decreases in mRNA expression of ENT1 and ENT2 in ENT1 cells (Figure 1D). Increase in [^{3}H]uridine uptake may be attributed to increased protein expression or function of the remaining functional transporter. However, we have not been able to find reliable antibodies for ENT1 and ENT2 to assess this.

There was a 13.8-fold difference in the K_t for ENT1 and ENT2 that aligns with observations in wild-type HeLa S3 cells (reported K_t of 13.6 μM and 108.9 μM, respectively) (Miller et al., 2020). NBMPR inhibited ENT1 with over 100-fold higher

Downloaded from molpharm.aspetjournals.org at ASPET Journals on April 16, 2024

Molecular Pharmacology Fast Forward. Published on December 1, 2020 as DOI: 10.1124/molpharm.120.000169
This article has not been copyedited and formatted. The final version may differ from this version.

affinity than ENT2, which complements previously reported values in our lab with wild-type HeLa cells and others using heterologous expression systems (Boleti et al., 1997; Miller et al., 2020; Plagemann et al., 1978; Plagemann and Wohlhueter, 1984; Ward et al., 2000). The data confirm that CRISPR/Cas9 functional knockout of natively expressed ENTs in HeLa cells result in transport activity of the remaining homology that retains quantitatively similar characteristics as those expressed in other natively expressing model systems.

In studies with endogenous nucleosides, cytidine had the highest affinity for ENT1, and inosine had the highest affinity for ENT2. Thymidine had a higher affinity for ENT1 than ENT2, whereas guanosine and adenosine did not have differences in affinity for each transporter, similar to previously reported values using wild-type HeLa cells and NBMPR (Miller et al., 2020). However, the authors did not observe a difference between the IC_{50} values of thymidine for ENT1 and ENT2 mediated [^{3}H]uridine uptake (Miller et al., 2020). These knockout cell lines assisted with the differentiation of this parameter for thymidine and could assist in delineating ENT1 or ENT2 affinity for other compounds.

In our studies with nucleoside reverse transcriptase inhibitors, abacavir inhibited both ENT1 and ENT2 mediated [^{3}H]uridine uptake, whereas zidovudine, entecavir and emtricitabine inhibited ENT2 at a lower concentration than ENT1. Abacavir and entecavir are both guanosine analogs, however, guanosine appears to be a relatively low affinity substrate for both ENT1 and ENT2 (Miller et. al., 2020). We previously

Downloaded from molpharm.aspetjournals.org at ASPET Journals on April 16, 2024

Molecular Pharmacology Fast Forward. Published on December 1, 2020 as DOI: 10.1124/molpharm.120.000169
This article has not been copyedited and formatted. The final version may differ from this version.

reported that abacavir is an inhibitor but not a substrate of the ENTs, with entry into HeLa cells limited to diffusion (Miller et al., 2020). The IC_{50} values determined in the present study for abacavir against ENT1- and ENT2-mediated [^{3}H]uridine uptake showed that abacavir has ~3.7-fold higher affinity for ENT1 than ENT2.

We expanded our investigation into ENT-drug interactions by testing thirty-seven nucleoside/heterocycle analogs. These compounds are structurally diverse and range in molecular weight from 225 to 735 g/mol. Seventeen compounds inhibited uptake in at least one of the cell lines: GS-9667, lexibulin, ticagrelor, GS-6620, darusentan, acalisib, GS-0938, GS-9191 uridine triacetate, clofarabine, cladribine, darunavir, nelarabine, nevirapine, eleclazine, mericitabine, and tecadenoson. Of the nucleoside/heterocycle analogs that inhibited uptake, 76% had a molecular weight over 300 g/mol. Of the nucleoside/heterocycle analogs that failed to inhibit uptake, 65% had a molecular weight below 300 g/mol. Based on this limited data set, it appears that inhibition of ENT activity correlates with increased molecular weight. GS-9667 was the most potent inhibitor of ENT1 (estimated-IC_{50} = ~4 μM), while GS-6620 was the most potent inhibitor of ENT2 (estimated-IC_{50} = ~14 μM). The large difference in affinity of ENT1 and ENT2 for NBMPR shows that these two homologous transporters (amino acid sequence identity of ~45%) have markedly different selectivity profiles. Here, we found that three compounds: nevirapine, ticagrelor, and uridine triacetate, had different inhibitory profiles for ENT1 and ENT2. Nevirapine more potently inhibited ENT2 than ENT1, and ticagrelor and uridine triacetate were more potent inhibitors of ENT1 than ENT2 (Figures 7 and 8B).

Downloaded from molpharm.aspetjournals.org at ASPET Journals on April 16, 2024

Molecular Pharmacology Fast Forward. Published on December 1, 2020 as DOI: 10.1124/molpharm.120.000169
This article has not been copyedited and formatted. The final version may differ from this version.

The ENTs are not included by the International Transporter Consortium (Consortium, 2010), the US Food and Drug Administration (Services, 2017), or the European Medicines Agency (Products, 2012) as transporter targets for unwanted drug-drug interactions (DDIs). Nevertheless, their recommendation that unbound C_{max}/IC_{50} ratios of $\geq$0.1 as indicators of potential unwanted DDIs suggests that interactions of ENT1 with abacavir (IC_{50} value of 85.7 μM and C_{max} of 2.23 – 15.3 μM (Hervey and Perry, 2000) produce a C_{max}/IC_{50} of 0.026 – 0.179 suggesting it could contribute to unwanted inhibition of transport of endogenous nucleosides.

The initial screening of the nucleoside/heterocycle analogs only identifies interactions and does not determine if these compounds are substrates or inhibitors of the ENTs. The classification of identified inhibitors of the ENTs was explored for nevirapine, lexibulin, clofarabine and cladribine. Transport of these compounds with and without 100 μM NBMPR was measured and detected by LC-MS/MS. Compounds without a decrease in uptake in the presence of NBMPR were concluded to be inhibitors at the tested concentration. Compounds with a decrease in uptake in the presence of NBMPR were classified as substrates. A decrease in clofarabine and cladribine uptake in the presence of NBMPR suggests both compounds are substrates (and competitive inhibitors of uridine uptake) of both transporters. No change in nevirapine uptake in the presence of NBMPR suggests that nevirapine is a non-transported inhibitor of both ENT1 and ENT2. No change in lexibulin uptake in the presence of NBMPR in ENT1 cells was observed suggesting it is a non-transported inhibitor of ENT1. An increase in

Downloaded from molpharm.aspetjournals.org at ASPET Journals on April 16, 2024

Molecular Pharmacology Fast Forward. Published on December 1, 2020 as DOI: 10.1124/molpharm.120.000169
This article has not been copyedited and formatted. The final version may differ from this version.

uptake in ENT2 cells in the presence of NBMPR suggests that lexibulin is also a non-transported inhibitor of ENT2. Further investigation into compounds that interact with the ENTs will classify compounds as substrates or inhibitors, and may reveal differences in substrate selectivity between ENT1 and ENT2.

We identified significant interactions with both ENT1 and ENT2 for clofarabine and cladribine, as have previous studies (King et al., 2005). Gemcitabine is a widely accepted substrate of the ENTs (Hammond et al., 1999; Hioki et al., 2018; Kim et al., 2018; Santini et al., 2011; Vincenzi et al., 2017). Although gemcitabine is a substrate, we observed modest inhibition of [^{3}H]uridine uptake in the presence of gemcitabine, consistent with other reports of gemcitabine inhibition of [^{3}H]uridine uptake (Hioki et al., 2018) (Shimada et al., 2015). Trifluridine is a reported substrate of both ENT1 and ENT2, and we observed modest interactions with ENT1 and ENT2 (Takahashi et al., 2018). Interestingly, cytarabine did not inhibit ENT1 activity and slightly inhibited ENT2 activity although cytarabine is a substrate of both transporters (Català et al., 2016; Clarke et al., 2006; White et al., 1987; Wiley et al., 1983). Modest interactions with azacitadine and ENT1 and with decitabine and ENT2 were identified, although previous studies report both compounds as substrates for both transporters (Arimany-Nardi et al., 2014; Damaraju et al., 2012; Hummel-Eisenbeiss et al., 2013).

Bayesian machine learning models have been successfully and widely used to predict chemical bioactivity and improve and facilitate the drug discovery process. Using the Assay Central® software, we generated predictive Bayesian models for inhibitors of

Downloaded from molpharm.aspetjournals.org at ASPET Journals on April 16, 2024

Molecular Pharmacology Fast Forward. Published on December 1, 2020 as DOI: 10.1124/molpharm.120.000169
This article has not been copyedited and formatted. The final version may differ from this version.

ENT1 and ENT2 (Lane et al., 2018; Russo et al., 2018; Zorn et al., 2019). These models of ENT1 and ENT2 inhibition performed well in five-fold cross-validation as demonstrated by internal receiver operator characteristic (ROC) scores greater than 0.7. Subvalidations based on the ENT1 training model built from IC_{50} data available from ChEMBL show that the model successfully predicted the majority of compounds that interact with ENT1. Using percent uptake, 58% of the inhibitors were correctly identified, and using estimated-IC_{50} values 63% of the inhibitors were correctly identified. Testing additional diverse compounds and generating true IC_{50} values for identified inhibitors of ENT1 and ENT2 will aid in improving the Bayesian models as tools for increasing the efficiency of drug development, as well as contributing to the generation of quantitative pharmacophores for these transporters.

In conclusion, the CRISPR/Cas9 system was used to produce HeLa cell lines that functionally expressed either ENT1 or ENT2, which were used to evaluate the impact of therapeutically relevant nucleoside-based compounds on transporter function. Moreover, these cell lines were crucial for the generation of predictive models for drug interactions with ENT1 and ENT2. There were marked differences in ENT1 and ENT2 selectivity with abacavir, nevirapine, ticagrelor, and uridine triacetate. Machine learning models based on these results can predict probable inhibitory interactions with the ENTs. Additionally, determining the structural differences in substrates for both transporters is essential in order for developing BTB-permeable compounds using the ENT1-ENT2 transepithelial transport pathway. Focused drug design informed by

Downloaded from molpharm.aspetjournals.org at ASPET Journals on April 16, 2024

Molecular Pharmacology Fast Forward. Published on December 1, 2020 as DOI: 10.1124/molpharm.120.000169
This article has not been copyedited and formatted. The final version may differ from this version.

machine learning models developed from substrate selectivity data has the potential to improve the disposition of drugs by ENTs to treat viral infections and cancer in the MGT.

Downloaded from molpharm.aspetjournals.org at ASPET Journals on April 16, 2024

Acknowledgements:

We thank Gilead Sciences Inc. (Foster City, CA) for providing us with selected compounds and Dr. Bill Smith for advice and review of the manuscript.

Authorship Contributions

Participated in research design: Miller, Jilek, Jennings, Galligan, Foil, Zorn, Ekins, Wright, Cherrington

Conducted experiments: Miller, Zhang, Hau, Jilek, Jennings, Foil, Zorn, Ekins

Performed data analysis: Miller, Zhang, Hau, Jilek, Jennings, Foil, Zorn, Ekins, Wright

Wrote or contributed to the writing of the manuscript: Miller, Zhang, Jilek, Hau, Jennings, Galligan, Foil, Zorn, Ekins, Wright and Cherrington

Molecular Pharmacology Fast Forward. Published on December 1, 2020 as DOI: 10.1124/molpharm.120.000169
This article has not been copyedited and formatted. The final version may differ from this version.

Downloaded from molpharm.aspetjournals.org at ASPET Journals on April 16, 2024

References

Arimany-Nardi, C., Errasti-Murugarren, E., Minuesa, G., Martinez-Picado, J., Gorboulev, V., Koepsell, H., and Pastor-Anglada, M. (2014). Nucleoside transporters and human organic cation transporter 1 determine the cellular handling of DNA-methyltransferase inhibitors. British Journal of Pharmacology *171*, 3868-3880.

Atlas, H. P. (2020). Human Protein Atlas available from http://www.proteinatlas.org. In.

Boleti, H., Coe, I. R., Baldwin, S. A., Young, J. D., and Cass, C. E. (1997). Molecular identification of the equilibrative NBMPR-sensitive (es) nucleoside transporter and demonstration of an equilibrative NBMPR-insensitive (ei) transport activity in human erythroleukemia (K562) cells. Neuropharmacology *36*, 1167-1179.

Molecular Pharmacology Fast Forward. Published on December 1, 2020 as DOI: 10.1124/molpharm.120.000169
This article has not been copyedited and formatted. The final version may differ from this version.

Boswell-Casteel, R. C., and Hays, F. A. (2017). Equilibrative nucleoside transporters—A review. Nucleosides, Nucleotides and Nucleic Acids *36*, 7-30.

Cardona Maya, W. D., Du Plessis, S. S., and Velilla, P. A. (2020). SARS-CoV-2 and the Testis: similarity to other viruses and routes of infection. Reproductive BioMedicine Online *40*, 763-764.

Carletta, J. (1996). Assessing agreement on classification tasks: The kappa statistic. Comput Linguist *22*, 249-254.

Català, A., Pastor-Anglada, M., Caviedes-Cárdenas, L., Malatesta, R., Rives, S., Vega-García, N., Camós, M., and Fernández-Calotti, P. (2016). FLT3 is implicated in cytarabine transport by human equilibrative nucleoside transporter 1 in pediatric acute leukemia. Oncotarget *7*, 49786-49799.

Clark, A. M., Dole, K., Coulon-Spektor, A., McNutt, A., Grass, G., Freundlich, J. S., Reynolds, R. C., and Ekins, S. (2015). Open Source Bayesian Models. 1. Application to ADME/Tox and Drug Discovery Datasets. Journal of Chemical Information and Modeling *55*, 1231-1245.

Clark, A. M., and Ekins, S. (2015). Open Source Bayesian Models. 2. Mining a "Big Dataset" To Create and Validate Models with ChEMBL. J Chem Inf Model *55*, 1246-1260.

Clarke, M. L., Damaraju, V. L., Zhang, J., Mowles, D., Tackaberry, T., Lang, T., Smith, K. M., Young, J. D., Tomkinson, B., and Cass, C. E. (2006). The Role of Human Nucleoside Transporters in Cellular Uptake of 4′-Thio-β-d-arabinofuranosylcytosine and β-d-Arabinosylcytosine. Molecular Pharmacology *70*, 303-310.

Downloaded from molpharm.aspetjournals.org at ASPET Journals on April 16, 2024

Molecular Pharmacology Fast Forward. Published on December 1, 2020 as DOI: 10.1124/molpharm.120.000169
This article has not been copyedited and formatted. The final version may differ from this version.

Cohen, J. (1960). A coefficient of agreement for nominal scales. Psychol Meas *20*, 37-46.

Cong, L., and Zhang, F. (2015). Genome Engineering Using CRISPR-Cas9 System. In, (Springer New York), pp. 197-217.

Dahlig-Harley, E., Eilam, Y., Paterson, A. R. P., and Cass, C. E. (1981). Binding of nitrobenzylthioinosine to high-affinity sites on the nucleoside-transport mechanism of HeLa cells. Biochem J *200*, 295-305.

Damaraju, V. L., Mowles, D., Yao, S., Ng, A., Young, J. D., Cass, C. E., and Tong, Z. (2012). Role of Human Nucleoside Transporters in the Uptake and Cytotoxicity of Azacitidine and Decitabine. Nucleosides, Nucleotides and Nucleic Acids *31*, 236-255.

Durmus, S., Hendrikx, J. J. M. A., and Schinkel, A. H. (2015). Chapter one- Apical ABC Transporters and Cancer Chemotherapeutic Drug Disposition. Adv Cancer Res *125*, 1-41.

Eastman, R. T., Roth, J. S., Brimacombe, K. R., Simeonov, A., Shen, M., Patnaik, S., and Hall, M. D. (2020). Remdesivir: A Review of Its Discovery and Development Leading to Emergency Use Authorization for Treatment of COVID-19. ACS Cent Sci, A-L.

European Medicines Agency Committee for Human Medicinal Products. (2012). Guideline on the investigation of drug interactions.

Ewald, B., Sampath, D., and Plunkett, W. (2008). Nucleoside analogs: molecular mechanisms signaling cell death. *27*, 6522-6537.

Downloaded from molpharm.aspetjournals.org at ASPET Journals on April 16, 2024

Molecular Pharmacology Fast Forward. Published on December 1, 2020 as DOI: 10.1124/molpharm.120.000169
This article has not been copyedited and formatted. The final version may differ from this version.

Gaffney, D. O., Jennings, E. Q., Anderson, C. C., Marentette, J. O., Shi, T., Schou Oxvig, A.-M., Streeter, M. D., Johannsen, M., Spiegel, D. A., Chapman, E.*, et al.* (2019). Non-enzymatic Lysine Lactoylation of Glycolytic Enzymes. Cell Chemical Biology.

Griffith, D. A., and Jarvis, S. M. (1996). Nucleoside and nucleobase transport systems of mammalian cells. Biochimica et Biophysica Acta *1286*, 153-181.

Hammond, J. R., Lee, S., and Ferguson, P. J. (1999). [3H]Gemcitabine Uptake By Nucleoside Transporters in a Human Head and Neck Squamous Carcinoma Cell Line. J Pharmacol Exp Ther *288*, 1185-1191.

Hervey, P. S., and Perry, C. M. (2000). Abacavir: A Review of its Clinical Potential in Patients with HIV Infection. Drugs *60*, 447-479.

Hioki, M., Shimada, T., Yuan, T., Nakanishi, T., Tajima, H., Yamazaki, M., Yokono, R., Takabayashi, M., Sawamoto, K., Akashita, G.*, et al.* (2018). Contribution of equilibrative nucleoside transporters 1 and 2 to gemcitabine uptake in pancreatic cancer cells. Biopharmaceutics & Drug Disposition *39*, 256-264.

Huber-Ruano, I., and Pastor-Anglada, M. (2009). Transport of Nucleoside Analogs Across the Plasma Membrane: A Clue to Understanding Drug-Induced Cytotoxicity. Curr Drug Metab *10*, 347-358.

Hummel-Eisenbeiss, J., Hascher, A., Hals, P.-A., Sandvold, M. L., Müller-Tidow, C., Lyko, F., and Rius, M. (2013). The Role of Human Equilibrative Nucleoside Transporter 1 on the Cellular Transport of the DNA Methyltransferase Inhibitors 5-Azacytidine and CP-4200 in Human Leukemia Cells. Molecular Pharmacology *84*, 438-450.

International Transporter Consortium. (2010). Membrane transporters in drug development. Nature Reviews Drug Discovery *9*, 215-236.

Downloaded from molpharm.aspetjournals.org at ASPET Journals on April 16, 2024

Molecular Pharmacology Fast Forward. Published on December 1, 2020 as DOI: 10.1124/molpharm.120.000169
This article has not been copyedited and formatted. The final version may differ from this version.

Jordan, P. C., Stevens, S. K., and Deval, J. (2018). Nucleosides for the treatment of respiratory RNA virus infections. Antiviral Chemistry and Chemotherapy *26*, 204020661876448.

Jordheim, L. P., Durantel, D., Zoulim, F., and Dumontet, C. (2013). Advances in the development of nucleoside and nucleotide analogues for cancer and viral diseases. Nature Reviews Drug Discovery *12*, 447-464.

Kato, R., Maeda, T., Akaike, T., and Tamai, I. (2005). Nucleoside transport at the blood-testis barrier studied with primary-cultured sertoli cells. J Pharmacol Exp Ther *312*, 601-608.

Kido, Y., Matsson, P. R., and Giacomini, K. M. (2011). Profiling of a Prescription Drug Library for Potential Renal Drug–Drug Interactions Mediated by the Organic Cation Transporter 2. Journal of Medicinal Chemistry *54*, 4548-4558.

Kim, J., Kim, H., Lee, J.-C., Kim, J. W., Paik, W. H., Lee, S. H., Hwang, J.-H., Ryu, J. K., and Kim, Y.-T. (2018). Human equilibrative nucleoside transporter 1 (hENT1) expression as a predictive biomarker for gemcitabine chemotherapy in biliary tract cancer. PLOS ONE *13*, e0209104.

King, K. M., Damaraju, V. L., Vickers, M. F., Yao, S. Y., Lang, T., Tackaberry, T. E., Mowles, D. A., Ng, A. M. L., Young, J. D., and Cass, C. E. (2005). A Comparison of the Transportability, and Its Role in Cytotoxicity, of Clofarabine, Cladribine, and Fludarabine by Recombinant Human Nucleoside Transporters Produced in Three Model Expression Systems. Molecular Pharmacology *69*, 346-353.

Klein, D. M., Evans, K. K., Hardwick, R. N., Dantzler, W. H., Wright, S. H., and Cherrington, N. J. (2013). Basolateral Uptake of Nucleosides by Sertoli Cells Is

Downloaded from molpharm.aspetjournals.org at ASPET Journals on April 16, 2024

Molecular Pharmacology Fast Forward. Published on December 1, 2020 as DOI: 10.1124/molpharm.120.000169
This article has not been copyedited and formatted. The final version may differ from this version.

Mediated Primarily by Equilibrative Nucleoside Transporter 1. J Pharmacol Exp Ther *346*, 121-129.

Koczor, C. A., Torres, R. A., and Lewis, W. (2012). The role of transporters in the toxicity of nucleoside and nucleotide analogs. Expert Opin Drug Metab Toxicol *8*, 665-676.

Lane, T., Russo, D. P., Zorn, K. M., Clark, A. M., Korotcov, A., Tkachenko, V., Reynolds, R. C., Perryman, A. L., Freundlich, J. S., and Ekins, S. (2018). Comparing and Validating Machine Learning Models for *Mycobacterium tuberculosis* Drug Discovery. Mol Pharmaceutics *15*, 4346-4360.

Lauzon G, P. A. (1977). Binding of the Nucleoside Transport Inhibitor Nitrobenzylthioinosine to HeLa Cells. Molecular Pharmacology *13*, 883-891.

Le Tortorec, A., and Dejucq-Rainsford, N. (2010). HIV infection of the male genital tract - consequences for sexual transmission and reproduction. *33*, e98-e108.

Li, D., Jin, M., Bao, P., Zhao, W., and Zhang, S. (2020). Clinical Characteristics and Results of Semen Tests Among Men With Coronavirus Disease 2019. JAMA Network Open *3*, e208292.

Livak, K., and Schmittgen, T. (2001). Analysis of Relative Gene Expression Data Using Real-Time Quantitative PCR and the 2−ΔΔCT Method. Methods *25*, 402-408.

Lucas, S., and Nelson, A. M. (2015). HIV and the spectrum of human disease. The Journal of Pathology *235*, 229-241.

Mackey, J. R., Yao, S. Y. M., Smith, K. M., Karpinski, E., Baldwin, S. A., Cass, C. E., and Young, J. D. (1999). Gemcitabine Transport in Xenopus Oocytes Expressing

Downloaded from molpharm.aspetjournals.org at ASPET Journals on April 16, 2024

Molecular Pharmacology Fast Forward. Published on December 1, 2020 as DOI: 10.1124/molpharm.120.000169
This article has not been copyedited and formatted. The final version may differ from this version.

Recombinant Plasma Membrane Mammalian Nucleoside Transporters. JNCI Journal of the National Cancer Institute *91*, 1876-1881.

Matthews, B. W. (1975). Comparison of the predicted and observed secondary structure of T4 phage lysozyme. Biochimica et Biophysica Acta (BBA) - Protein Structure *405*, 442-451.

Miller, S. R., and Cherrington, N. J. (2018). Transepithelial transport across the blood-testis barrier. Reproduction *156*, R187-R194.

Miller, S. R., Hau, R. K., Jilek, J. L., Morales, M. N., Wright, S. H., and Cherrington, N. J. (2020). Nucleoside Reverse Transcriptase Inhibitor (NRTI) Interaction with Human Equilibrative Nucleoside Transporters 1 and 2. Drug Metab Dispos *48*.

Mruk, D. D., and Cheng, C. Y. (2015). The Mammalian Blood-Testis Barrier: Its Biology and Regulation. Endocrine Reviews *36*, 564-591.

Mruk, D. D., Su, L., and Cheng, C. Y. (2011). Emerging role for drug transporters at the blood-testis barrier. Trends Pharmacol Sci *32*, 99-106.

Pastor-Anglada, M., and Pérez-Torras, S. (2015). Nucleoside transporter proteins as biomarkers of drug responsiveness and drug targets. Front Pharmacol *6*, 1-14.

Plagemann, P. G. W., Marz, R., and Wohlhueter, R. M. (1978). Uridine transport in novikoff rat hepatoma cells and other cell lines and its relationship to uridine phosphorylation and phosphorolysis. *97*, 49-72.

Plagemann, P. G. W., and Wohlhueter, R. M. (1984). Nucleoside transport in cultured mammalian cells multiple forms with different sensitivity to inhibition by nitrobenzylthioinosine or hypoxanthine. *773*, 39-52.

Downloaded from molpharm.aspetjournals.org at ASPET Journals on April 16, 2024

Molecular Pharmacology Fast Forward. Published on December 1, 2020 as DOI: 10.1124/molpharm.120.000169
This article has not been copyedited and formatted. The final version may differ from this version.

Ran, F. A., Hsu, P. D., Wright, J., Agarwala, V., Scott, D. A., and Zhang, F. (2013). Genome engineering using the CRISPR-Cas9 system. Nature Protocols *8*, 2281-2308.

Rehan, S., Shahid, S., Salminen, T. A., Jaakola, V.-P., and Paavilainen, V. O. (2019). Current Progress on Equilibrative Nucleoside Transporter Function and Inhibitor Design. SLAS DISCOVERY: Advancing Life Sciences R&D, 247255521987012.

Rozen, S., and Skaletsky, H. (2000). Primer3 on the WWW for General Users and for Biologist Programmers. Methods Mol Biol *132*, 365-386.

Russo, D. P., Zorn, K. M., Clark, A. M., Zhu, H., and Ekins, S. (2018). Comparing Multiple Machine Learning Algorithms and Metrics for Estrogen Receptor Binding Prediction. Molecular Pharmaceutics *15*, 4361-4370.

Sandoval, P. J., Zorn, K. M., Clark, A. M., Ekins, S., and Wright, S. H. (2018). Assessment of Substrate-Dependent Ligand Interactions at the Organic Cation Transporter OCT2 Using Six Model Substrates. Molecular Pharmacology *94*, 1057-1068.

Santini, D., Schiavon, G., Vincenzi, B., E. Cass, C., Vasile, E., D. Manazza, A., Catalano, V., G. Baldi, G., Lai, R., Rizzo, S*., et al.* (2011). Human Equilibrative Nucleoside Transporter 1 (hENT1) Levels Predict Response to Gemcitabine in Patients With Biliary Tract Cancer (BTC). Current Cancer Drug Targets *11*, 123-129.

Shimada, T., Nakanishi, T., Tajima, H., Yamazaki, M., Yokono, R., Takabayashi, M., Shimada, T., Sawamoto, K., Miyamoto, K.-I., Kitagawa, H*., et al.* (2015). Saturable Hepatic Extraction of Gemcitabine Involves Biphasic Uptake Mediated by Nucleoside Transporters Equilibrative Nucleoside Transporter 1 and 2. *104*, 3162-3169.

Downloaded from molpharm.aspetjournals.org at ASPET Journals on April 16, 2024

Molecular Pharmacology Fast Forward. Published on December 1, 2020 as DOI: 10.1124/molpharm.120.000169
This article has not been copyedited and formatted. The final version may differ from this version.

Sundaram, M. (2001). Topology of a Human Equilibrative, Nitrobenzylthioinosine (NBMPR)-sensitive Nucleoside Transporter (hENT1) Implicated in the Cellular Uptake of Adenosine and Anti-cancer Drugs. *276*, 45270-45275.

Takahashi, K., Yoshisue, K., Chiba, M., Nakanishi, T., and Tamai, I. (2018). Contribution of equilibrative nucleoside transporter(s) to intestinal basolateral and apical transports of anticancer trifluridine. Biopharmaceutics & Drug Disposition *39*, 38-46.

United States Department of Health and Human Services. (2017). In Vitro Metabolism and Transporter-Mediated Drug-Drug Interaction Studies Guidance for Industry Draft Guidance. In, Food and Drug Administration Center for Drug Evaluation and Research. Research, ed.

Vincenzi, B., Stacchiotti, S., Collini, P., Pantano, F., Rabitti, C., Perrone, G., Iuliani, M., Baldi, A., Badalamenti, G., Sanfilippo, R.*, et al.* (2017). Human equilibrative nucleoside transporter 1 gene expression is associated with gemcitabine efficacy in advanced leiomyosarcoma and angiosarcoma. British Journal of Cancer *117*, 340-346.

Ward, J. L., Sherali, A., Mo, Z. P., and Tse, C. M. (2000). Kinetic and pharmacological properties of cloned human equilibrative nucleoside transporters, ENT1 and ENT2, stably expressed in nucleoside transporter-deficient PK15 cells. Ent2 exhibits a low affinity for guanosine and cytidine but a high affinity for inosine. J Biol Chem *275*, 8375-8381.

White, J. C., Rathmell, J. P., and Capizzi, R. L. (1987). Membrane transport influences the rate of accumulation of cytosine arabinoside in human leukemia cells. Journal of Clinical Investigation *79*, 380-387.

Downloaded from molpharm.aspetjournals.org at ASPET Journals on April 16, 2024

Molecular Pharmacology Fast Forward. Published on December 1, 2020 as DOI: 10.1124/molpharm.120.000169
This article has not been copyedited and formatted. The final version may differ from this version.

Wiley, J. S., Jones, S. P., and Sawyer, W. H. (1983). Cytosine arabinoside transport by human leukaemic cells. European Journal of Cancer and Clinical Oncology *19*, 1067-1074.

Yao, S. Y., Ng, A. M., Sundaram, M., Cass, C. E., Baldwin, S. A., and Young, J. D. (2001). Transport of antiviral 3'-deoxy-nucleoside drugs by recombinant human and rat equilibrative, nitrobenzylthioinosine (NBMPR)-insensitive (ENT2) nucleoside transporter proteins produced in Xenopus oocytes. Mol Membr Biol *18*, 161-167.

Zorn, K. M., Lane, T. R., Russo, D. P., Clark, A. M., Makarov, V., and Ekins, S. (2019). Multiple Machine Learning Comparisons of HIV Cell-based and Reverse Transcriptase Data Sets. Molecular Pharmaceutics.

Downloaded from molpharm.aspetjournals.org at ASPET Journals on April 16, 2024

Footnotes

Funding:

This work was supported by the National Institutes of Health National Institute of General Medical Sciences [R01GM123643], the National Institutes of Health National Institute of Environmental Health Sciences [5P30ES006694, 2T32ES007091-36A1].

Molecular Pharmacology Fast Forward. Published on December 1, 2020 as DOI: 10.1124/molpharm.120.000169
This article has not been copyedited and formatted. The final version may differ from this version.

Downloaded from molpharm.aspetjournals.org at ASPET Journals on April 16, 2024

Figure Legends

Figure 1: Characterization of ENT1 and ENT2 KO Cell Lines. A) Location of deletion in SLC29A1 exon 5 (red “x”) and gRNA used for generation of the ENT1 KO (ENT2) cells. B) Location of deletion in SLC29A2 in exon 1 (red “X”) and gRNA used for generation of the ENT2 KO (ENT1) cells. DNA sequence 5’ to 3’ is shown for A) and B), as well as the amino acid sequence. C) Growth curve of wild-type HeLa S3 cells, and ENT1 and ENT2 cells. Log10 transformed cell growth data is also plotted. Total cell count data was analyzed using 2-way ANOVA with Sidak’s multiple comparisons test (* $p<0.05$, **

Molecular Pharmacology Fast Forward. Published on December 1, 2020 as DOI: 10.1124/molpharm.120.000169
This article has not been copyedited and formatted. The final version may differ from this version.

p<0.005, indicating difference from wild-type HeLa S3 cells). Data are presented as mean ± S.D. with *n=2* in duplicate. D) Real-time PCR mRNA expression of ENT1 and ENT2 in ENT knockout cells relative to wild-type HeLa S3 cells. Relative ENT1 expression (red) and relative ENT2 expression (blue). Data are presented as mean ± S.D. with *n=3* in duplicate.

Figure 2: Inhibition of [^{3}H]uridine uptake in ENT2 and ENT1 knockout cell lines. Approximately 20 nM [^{3}H]uridine was incubated with of 5 mM uridine (black square), 100 nM NBMPR (red triangle) or 100 μM NBMPR (blue triangle) in the ENT1 cell line (ENT2 KO, A) and the ENT2 (ENT1 KO, B) up to seven minutes. Total accumulated [^{3}H]uridine was measured. Data are represented as mean ± S.D. with *n=3* in triplicate.

Figure 3: NBMPR IC_{50} curves in ENT1 and ENT2 cell lines. Approximately 20 nM [^{3}H]uridine was incubated with increasing concentrations of NBMPR. Total accumulated [^{3}H]uridine was measured after two minutes. Results were normalized to total accumulated [^{3}H]uridine in the absence of NBMPR. Equation 2 was used to generate IC_{50} values for each experiment. Data are represented as mean ± S.D. with *n=3* in triplicate.

Figure 4: Uridine kinetics in ENT1 and ENT2 cell lines. 20 nM [^{3}H]uridine uptake in the presence of increasing amounts of unlabeled uridine was measured after two minutes. Michaelis-Menten kinetics (Equation 3) were used to generate kinetic parameters in

Downloaded from molpharm.aspetjournals.org at ASPET Journals on April 16, 2024

Molecular Pharmacology Fast Forward. Published on December 1, 2020 as DOI: 10.1124/molpharm.120.000169
This article has not been copyedited and formatted. The final version may differ from this version.

Table 2. The non-saturable component was subtracted from total accumulated [^{3}H]uridine. Data are represented as mean ± S.D. with *n=3* in triplicate.

Figure 5: Endogenous nucleoside [^{3}H]uridine uptake in ENT1 and ENT2 cell lines. Inhibition of [^{3}H]uridine uptake in the presence of endogenous nucleosides in ENT1 (blue squares) and ENT2 (red circles) cell lines. Equation 2 was used to generate best fit lines and IC_{50} values reported in Table 3. All data are represented as mean ± S.D. with *n=3* in triplicate.

Figure 6: NRTI inhibition of [^{3}H]uridine uptake in ENT1 and ENT2 cell lines. Approximately 20 nM of [^{3}H]uridine uptake was incubated with 100 μM (red bars), 300 μM (blue bars) or 1 mM (white bars) of nine different NRTIs for two minutes with ENT1 (A) or ENT2 (B) cell lines. The black bar represents tracer 20 nM [^{3}H]uridine only. Amount of [^{3}H]uridine uptake was normalized to percentage of uptake in tracer only condition. Ordinary one-way analysis of variance (ANOVA) with Bonferroni's correction for multiple comparisons to a control column (i.e. [^{3}H]uridine only) with 3 comparisons per family and *p<0.05, ** p<0.01, *** p<0.0001 was used.

Figure 7: Nucleoside/heterocycle analog inhibition of ENT-mediated [^{3}H]uridine uptake in ENT1 and ENT2 cell lines. Structures are provided in Supplemental Figure 1. Approximately 20 nM of [^{3}H]uridine was incubated with 200 μM of 37 different nucleoside/heterocycle analogs (white bars) for two minutes in each cell line. The black

Downloaded from molpharm.aspetjournals.org at ASPET Journals on April 16, 2024

Molecular Pharmacology Fast Forward. Published on December 1, 2020 as DOI: 10.1124/molpharm.120.000169
This article has not been copyedited and formatted. The final version may differ from this version.

bars represent 200 μM endogenous nucleosides, 100 nM NBMPR and 100 μM NBMPR. Ordinary one-way ANOVA with Dunnett 's correction for multiple comparisons ($p<0.05$ indicating a difference from control) was used for statistical analyses of these experiments. Significance is indicated by the compound name on the y axis (* $p<0.05$, ** $p<0.01$, *** $p<0.001$). Data is represented as mean ± S.D from duplicate values with *n=3.*

Figure 8:

Inhibition of [^{3}H]uridine uptake in the presence of abacavir (A), nevirapine (B), lexibulin (C), clofarabine (D), and cladribine (E) in ENT1 (red circles) and ENT2 (blue squares) cell lines. IC_{50} values are reported in Table 4. Data are reported as mean [^{3}H]uridine uptake as a percentage of control (i.e. in absence of compound) ± S.D. with *n=3* in duplicate.

Figure 9:

Determination of transport for identified inhibitors of [^{3}H]uridine uptake in ENT1 and ENT2 cell lines. Total accumulation of clofarabine (AB), cladribine (CD), lexibulin (EF) and nevirapine (GH) over five minutes measured in the absence and presence of 100 μM NBMPR in ENT cells detected by LC-MS/MS. 50 μM lexibulin, clofarabine, and cladribine were used for both cell lines, and nevirapine for ENT2 cells. 100 μM nevirapine was used for ENT1 cells. Data are reported as mean ± S.D. with *n=3* in duplicate.

Downloaded from molpharm.aspetjournals.org at ASPET Journals on April 16, 2024

Molecular Pharmacology Fast Forward. Published on December 1, 2020 as DOI: 10.1124/molpharm.120.000169
This article has not been copyedited and formatted. The final version may differ from this version.

Figure 10: ROC graphs generated from Assay Central® machine learning models for ENT1 and ENT2. The x-axis is the false positive rate, and the y-axis is the true positive rate. Bayesian models for ENT1 (A) and ENT2 (B). Models were created using the nucleoside/heterocycle analogs in Figure 7 and endogenous nucleosides. Predictions were evaluated using a standard probability cut off at 0.5, where a value greater than 0.5 was considered active. Compounds were further classified as active if the inhibition of uridine uptake was greater than 50%. Truth tables showing the number of false positive, false negative, true positive, and true negative inhibitors are included. Other statistical parameters including precision, recall, specificity, F1 score, Kappa, and MCC are defined.

Figure 11: ROC graphs generated from Assay Central® machine learning models for ENT1 using the ChEMBL dataset. The x-axis is the false positive rate, and the y-axis is the true positive rate. The ENT1 training model (A) was built from all IC_{50} data available from ChEMBL Target ID 1997 (https://www.ebi.ac.uk/chembl/target_report_card/CHEMBL1997/) and the threshold was set at 100 μM. The percent uptake subvalidation (B) test was defined by binary classification of percent uptake < 50% with 40 compounds total. The estimated-IC_{50} values subvalidation (C) test was defined by binary classification of estimated -IC_{50} values of less than 100 μM with 27 compounds total. Truth tables showing the number of false positive, false negative, true positive, and true negative inhibitors are included.

Downloaded from molpharm.aspetjournals.org at ASPET Journals on April 16, 2024

Molecular Pharmacology Fast Forward. Published on December 1, 2020 as DOI: 10.1124/molpharm.120.000169
This article has not been copyedited and formatted. The final version may differ from this version.

Other statistical parameters including precision, recall, specificity, F1 score, Kappa, and MCC are defined.

Table Legends

Table 1: Kinetic parameters of ENT2 and ENT1 knockout cell lines. An unpaired t-test was used to determine significance ($p<0.05$). All data are represented as mean ± S.D. with *n=3.*

Table 2: IC_{50} values of endogenous nucleosides in ENT1 and ENT2 cell lines. Best-fit values from Equation 2 were compared using the extra-sum of squares F-test to determine significance. IC_{50} values are represented as mean and 95% C.I. with *n=3.*

Table 3:

Estimated -IC_{50} values of nucleoside/heterocycle analogs that inhibited [^{3}H]Uridine uptake in ENT1 and ENT2 cell lines. Endogenous nucleoside estimated-IC_{50} values are also included. Values are ranked from lowest to highest in the ENT1 cells. IC_{50} values were generated from two data points: tracer only (0 μM) and 200 μM using Equation 4. A comparison of fits for the IC_{50} equation extra sum-of-squares F-test was done to compare the estimated-IC_{50} values for each cell line ($p<0.05$). Estimated-IC_{50} values are presented as mean and 95% C.I. with *n=3.*

Table 4:

Downloaded from molpharm.aspetjournals.org at ASPET Journals on April 16, 2024

Molecular Pharmacology Fast Forward. Published on December 1, 2020 as DOI: 10.1124/molpharm.120.000169
This article has not been copyedited and formatted. The final version may differ from this version.

IC_{50} values of abacavir, nevirapine, lexibulin, clofarabine and cladribine in ENT1 and ENT2 cell lines. Best-fit values from Equation 2 were compared using the extra-sum of squares F-test. IC_{50} values presented as mean and 95% C.I. with *n=3.*

Downloaded from molpharm.aspetjournals.org at ASPET Journals on April 16, 2024

Tables

1

Molecular Pharmacology Fast Forward. Published on December 1, 2020 as DOI: 10.1124/molpharm.120.000169
This article has not been copyedited and formatted. The final version may differ from this version.

	ENT1 Uridine Uptake	ENT2 Uridine Uptake	P Value	Ratio ENT2:ENT1
J_{max} (pmol•cm^{-2}•min^{-1})	23.75 ± 0.88	44.88 ± 16.34	p=0.089	1.89
K_t (μM)	11.36 ± 3.87	156.90 ± 55.60	p=0.016	13.81

Downloaded from molpharm.aspetjournals.org at ASPET Journals on April 16, 2024

Molecular Pharmacology Fast Forward. Published on December 1, 2020 as DOI: 10.1124/molpharm.120.000169
This article has not been copyedited and formatted. The final version may differ from this version.

Nucleoside	**ENT1 IC_{50} (μM)**	**ENT2 IC_{50} (μM)**	**P value**	**Ratio ENT2:ENT1**
Adenosine	**39.92** (95% CI: 24.5, 65.1)	**56.55** (95% CI: 29.3, 108.5)	p=0.377	1.42
Guanosine	**385.90** (95% CI: 194.4, 780.5)	**254.90** (95% CI: 140.5, 458.6)	p=0.358	0.66
Thymidine**	**708.90** 95% CI: (368.6, 1468)	**138.10** (95% CI: 64.7, 290.4)	p=0.0014	0.19
Inosine***	**219.50** (95% CI: 113.1, 426.4)	**27.02** (95% CI: 19.5, 37.49)	p<0.0001	0.12
Cytidine***	**21.08** (95% CI: 12.2, 36.7)	**368.20** (95% CI: 105.3, 1338)	p<0.0001	17.47

2

Downloaded from molpharm.aspetjournals.org at ASPET Journals on April 16, 2024

Molecular Pharmacology Fast Forward. Published on December 1, 2020 as DOI: 10.1124/molpharm.120.000169
This article has not been copyedited and formatted. The final version may differ from this version.

3

Analog	**ENT1 Estimated-IC_{50} (μM)**	**ENT2 Estimated-IC_{50} (μM)**	**Ratio ENT2:ENT1**
GS-9667	**4.3** (95% CI: -18.87, 34.45)	**24.0** (95% CI: -15.9, 89.22)	5.58
Lexibulin	**12.0** (95% CI: -13.4, 46.1)	**35.3** (95% CI: -16.8, 139.2)	2.94
Ticagrelor*	**12.4** (95% CI: -12.4, 45.2)	**441.1** (95% CI: 128.1, infinity)	35.57
GS-6620	**12.7** (95% CI: -14.2, 49.4)	**14.2** (95% CI: -24.5, 77.2)	1.12
Darusentan	**19.9** (95% CI: -8.6, 59.3)	**55.5** (95% CI: -4.2, 185.9)	2.79
Acalisib	**27.1** (95% CI: -2.8, 69.3)	**20.6** (95% CI: -17.9, 82.6)	0.76
GS-0938	**28.0** (95% CI: -3.3, 72.8)	**15.4** (95% CI: -18.4, 66.1)	0.55
Uridine Triacetate*	**28.4** (95% CI: -0.5, 68.5)	**228.7** (95% CI: 102.3, 656.0)	8.05
Clofarabine	**42.2** (95% CI: 10.7,87.0)	**54** (95% CI: 0.44, 159.2)	1.28
Cladribine	**66.1** (95% CI: 23.3, 135.1)	**35.7** (95% CI: -9.8, 116.2)	0.54
Darunavir	**68.8** (95% CI: 11.9, 182.2)	**15.8** (95% CI: -21.8, 75.69)	0.23
GS-9191	**180.4** (95% CI: 30.39, 1723)	**391.1** (95% CI: 108.8, infinity)	2.17
Nelarabine	**186.3** (95% CI: 15.9, 3480)	**225.2** (95% CI: 99.0, 659.3)	1.21
Nevirapine*	**198.3** (95% CI: 100.8, 434.4)	**23.7** (95% CI: -14.7, 85.3)	0.12
Eleclazine	**207.6** (95% CI: 47.5, 2934)	**222.6** (95% CI: 60.96, 2107)	1.07
Mericitabine	**209.8** (95% CI: 41.31, 11447)	**78.1** (95% CI: 16.2, 209.4)	0.37
Tecadenoson	**245.9** (95% CI: 52.7, infinity)	**171.8** (95% CI: 65.7, 510.7)	0.70
Adenosine	**194.1** (95% CI: 112.3, 357.0)	**80.2** (95% CI: 19.4, 205.9)	0.41
Guanosine	**646.9** (95% CI: 250.2, infinity)	**830.2** (95% CI: -infinity, infinity)	1.28

Downloaded from molpharm.aspetjournals.org at ASPET Journals on April 16, 2024

Molecular Pharmacology Fast Forward. Published on December 1, 2020 as DOI: 10.1124/molpharm.120.000169
This article has not been copyedited and formatted. The final version may differ from this version.

Thymidine*	**624.4** (95% CI: 221.6, infinity)	**126.0** (95% CI: 43.4, 338.0)	0.20
Inosine*	**394.0** (95% CI: 182.0, 1601.0)	**100.0** (95% CI: 34.3, 238.5)	0.25
Cytidine*	**25.6** (95% CI: -3.2, 65.5)	**507.9** (95% CI: 209.2, 7457)	19.84

Downloaded from molpharm.aspetjournals.org at ASPET Journals on April 16, 2024

Molecular Pharmacology Fast Forward. Published on December 1, 2020 as DOI: 10.1124/molpharm.120.000169
This article has not been copyedited and formatted. The final version may differ from this version.

4

Nucleoside	**ENT1 IC_{50} (μM)**	**ENT2 IC_{50} (μM)**	**P Value**	**Ratio ENT2:ENT1**
Abacavir**	**85.74** (95% CI: 34.22,137.3)	**316.8** (95% CI: 113.3, 520.2)	p=0.0056	3.69
Nevirapine*	**166.8** (95% CI: -32.88, 366.6)	**17.78** (95% CI: 2.83, 32.73)	p=0.0113	0.11
Lexibulin	**16.49** (95% CI: 0.776, 32.20)	**21.32** (95% CI: -2.24, 44.89)	p=0.722	1.29
Clofarabine	**31.48** (95% CI: 11.83, 51.13)	**12.22** (95% CI: 2.53, 21.91)	p=0.0509	0.39
Cladribine	**67.26** (95% CI: 28.1, 106.4)	**40.15** (95% CI: 15.06, 65.24)	p=0.1703	0.60

Downloaded from molpharm.aspetjournals.org at ASPET Journals on April 16, 2024

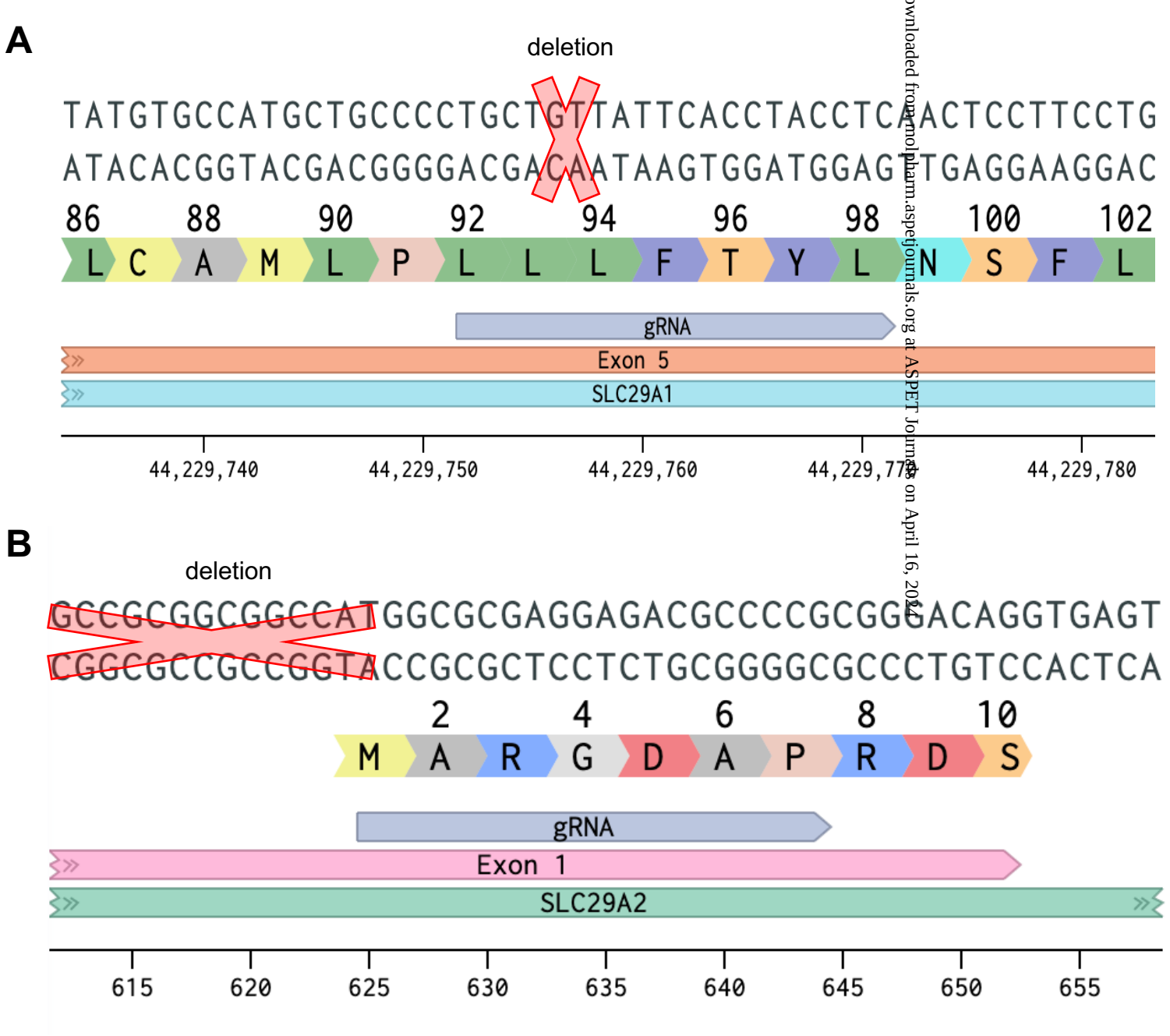

Downloaded from molpharm.aspetjournals.org at ASPET Journals on April 16, 2024

Figures 1A and 1B

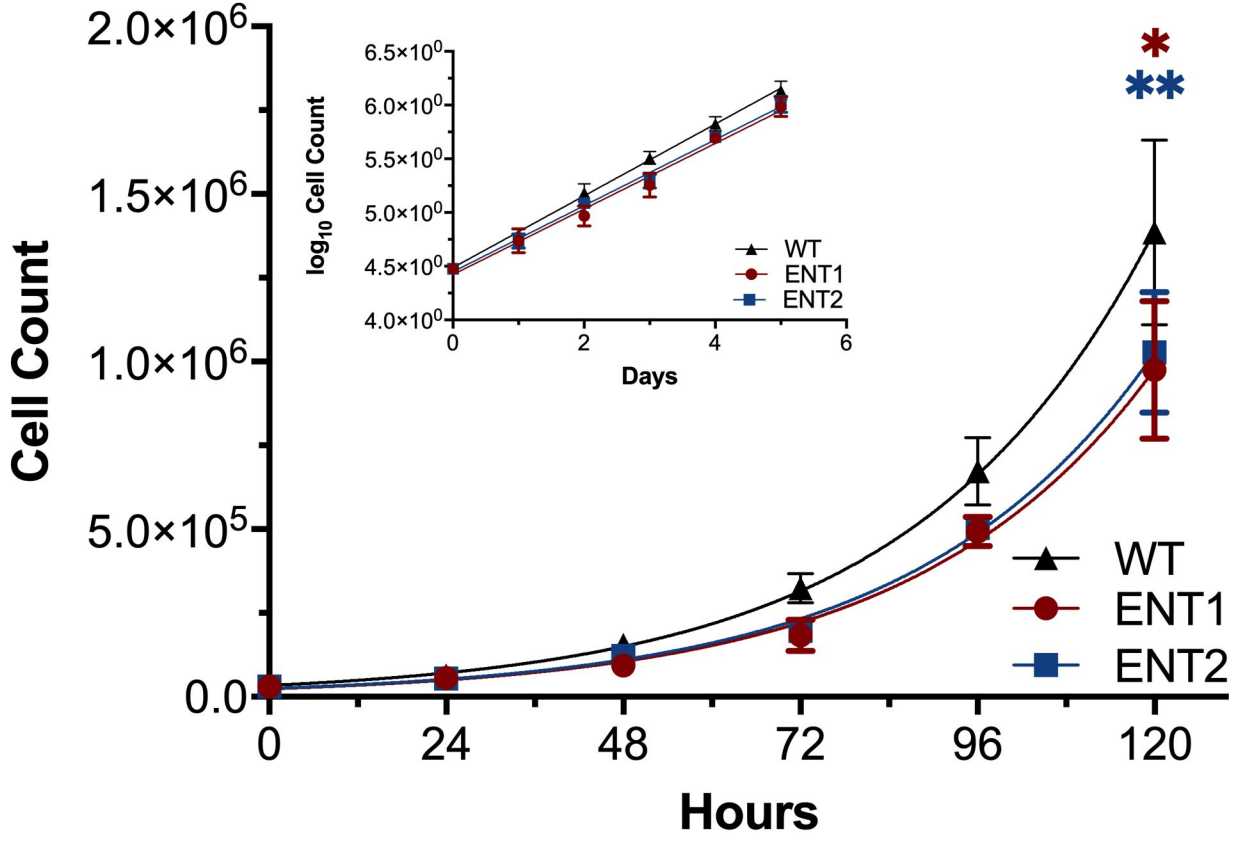
Cell Count
2.0×10^6
1.5×10^6
1.0×10^6
5.0×10^5
0.0
0
24
48
72
96
120
Hours
*
**
WT
ENT1
ENT2
log10 Cell Count
6.5×10^0
6.0×10^0
5.5×10^0
5.0×10^0
4.5×10^0
4.0×10^0
0
2
4
6
Days
WT
ENT1
ENT2

Figure 1C

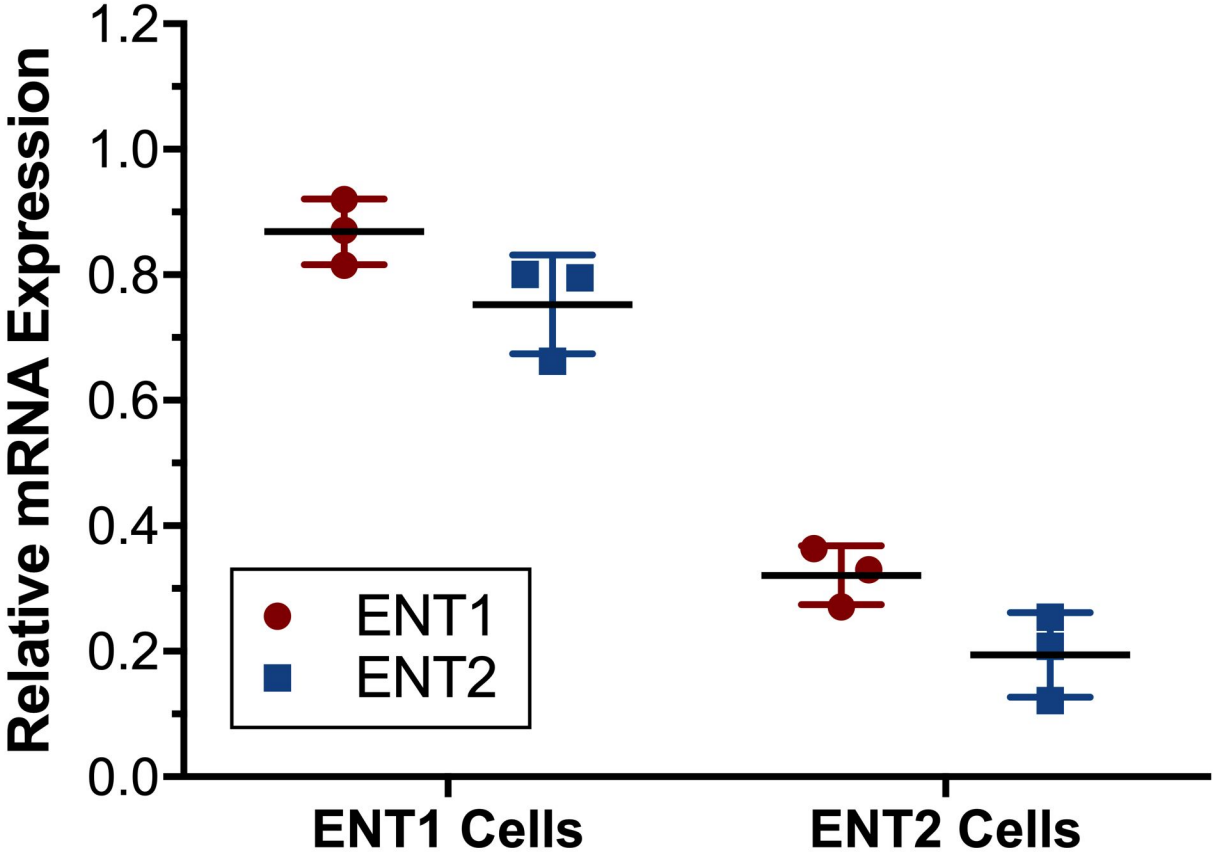
Relative mRNA Expression
1.2
1.0
0.8
0.6
0.4
0.2
0.0
ENT1
ENT2
ENT1 Cells
ENT2 Cells

Figure 1D

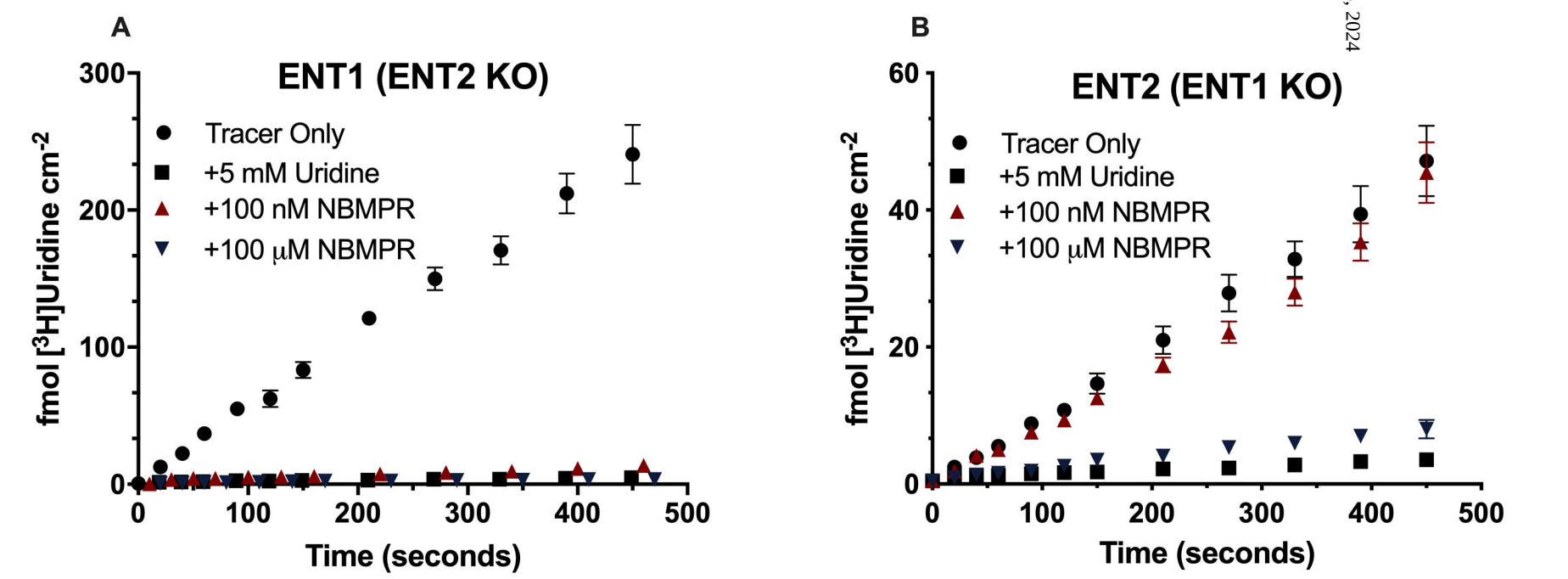
A
ENT1 (ENT2 KO)
Tracer Only
+5 mM Uridine
+100 nM NBMPR
+100 μM NBMPR
fmol [3H]Uridine cm-2
Time (seconds)
0
100
200
300
400
500
B
ENT2 (ENT1 KO)
Tracer Only
+5 mM Uridine
+100 nM NBMPR
+100 μM NBMPR
fmol [3H]Uridine cm-2
Time (seconds)
0
20
40
60

Figure 2

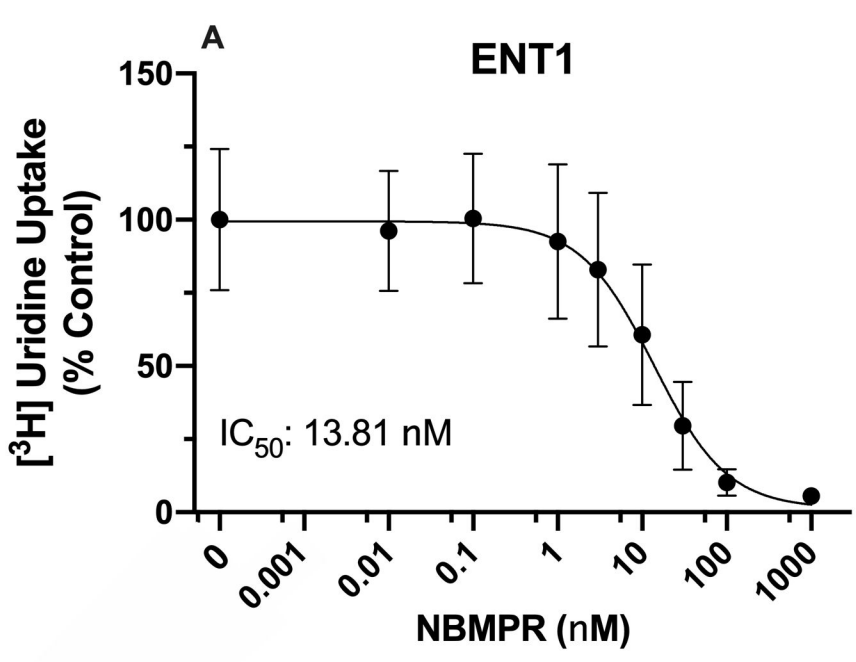

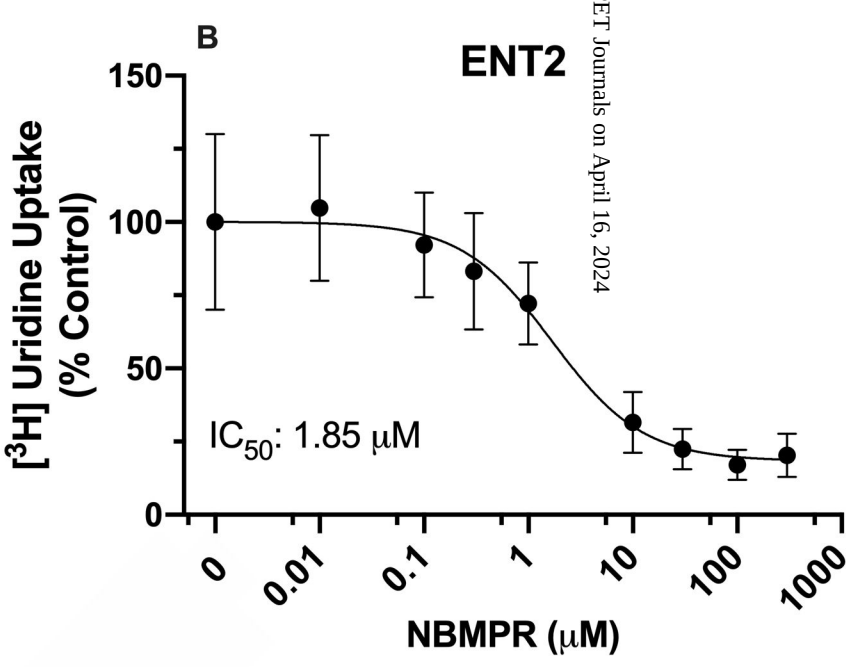

ET Journals on April 16, 2024

Figure 3

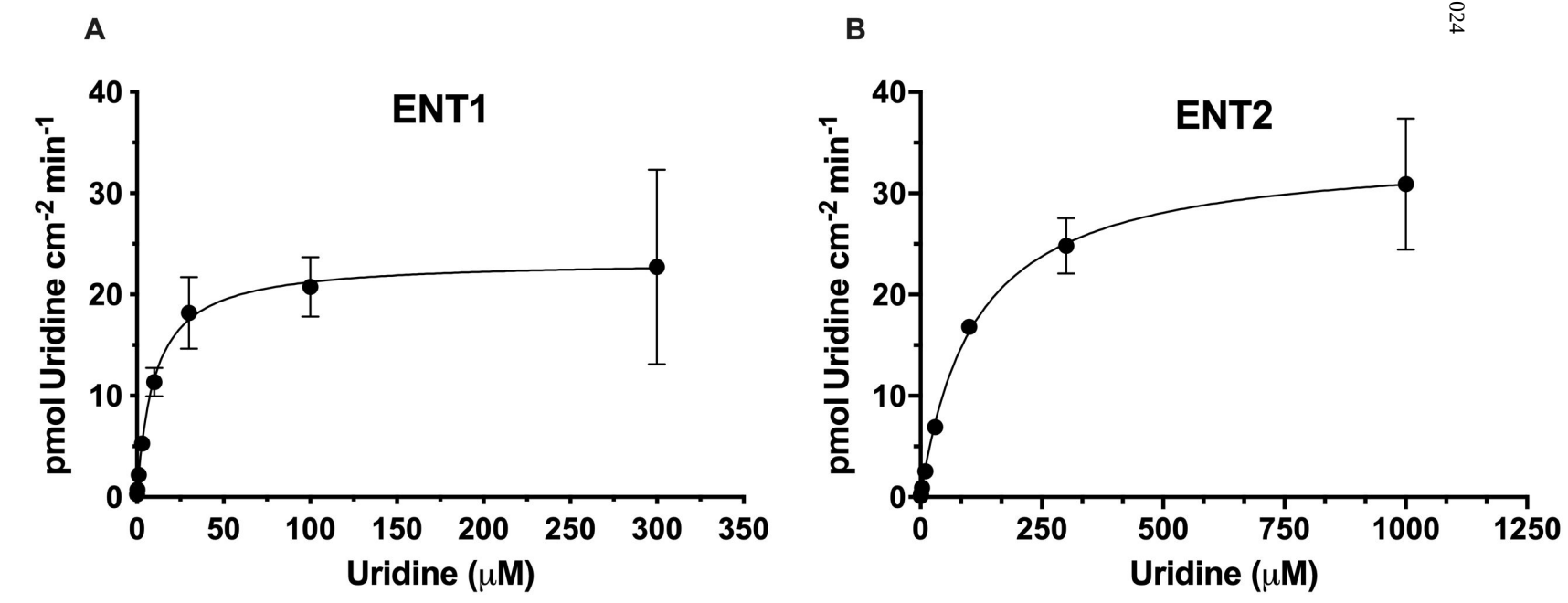
A
ENT1
pmol Uridine cm-2 min-1
0
10
20
30
40
0
50
100
150
200
250
300
350
Uridine (μM)
B
ENT2
pmol Uridine cm-2 min-1
0
10
20
30
40
0
250
500
750
1000
1250
Uridine (μM)

Figure 4

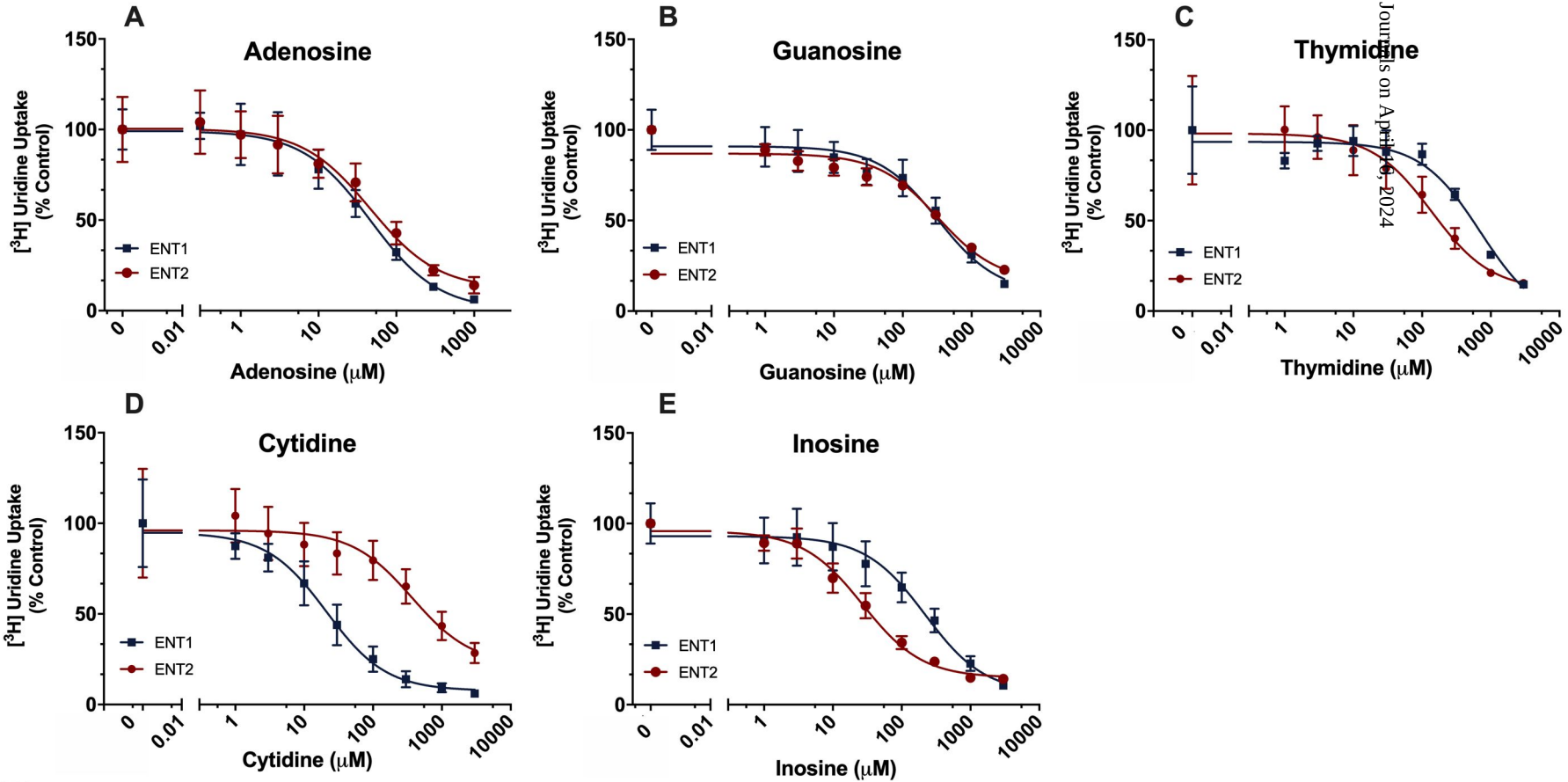

T Journals on April 16, 2024

Figure 5

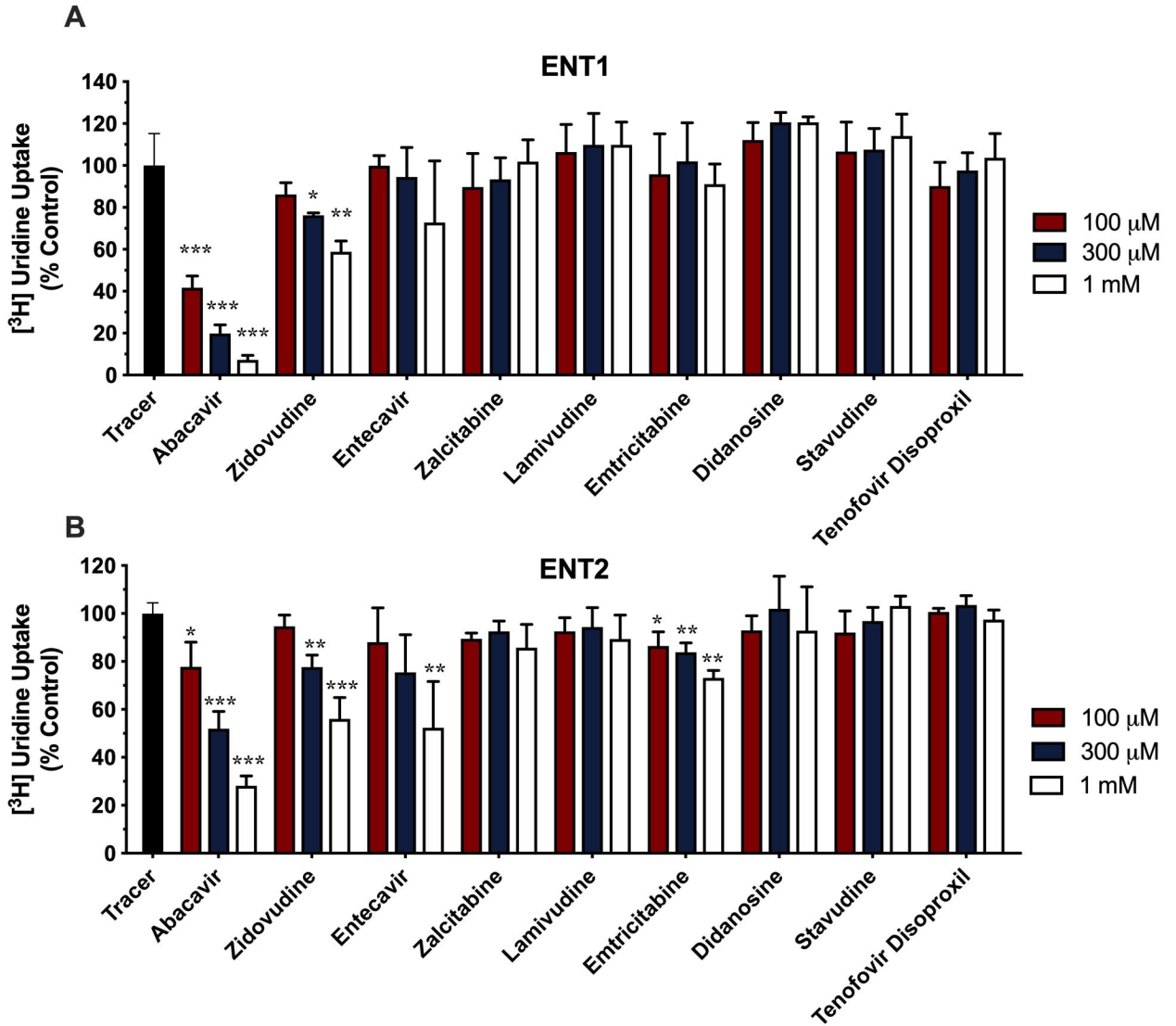
A
ENT1
[3H] Uridine Uptake (% Control)
140
120
100
80
60
40
20
0
***
***
***
*
**
100 μM
300 μM
1 mM
Tracer
Abacavir
Zidovudine
Entecavir
Zalcitabine
Lamivudine
Emtricitabine
Didanosine
Stavudine
Tenofovir Disoproxil
B
ENT2
[3H] Uridine Uptake (% Control)
120
100
80
60
40
20
0
*
***
***
**
***
**
*
**
**
100 μM
300 μM
1 mM
Tracer
Abacavir
Zidovudine
Entecavir
Zalcitabine
Lamivudine
Emtricitabine
Didanosine
Stavudine
Tenofovir Disoproxil

Figure 6

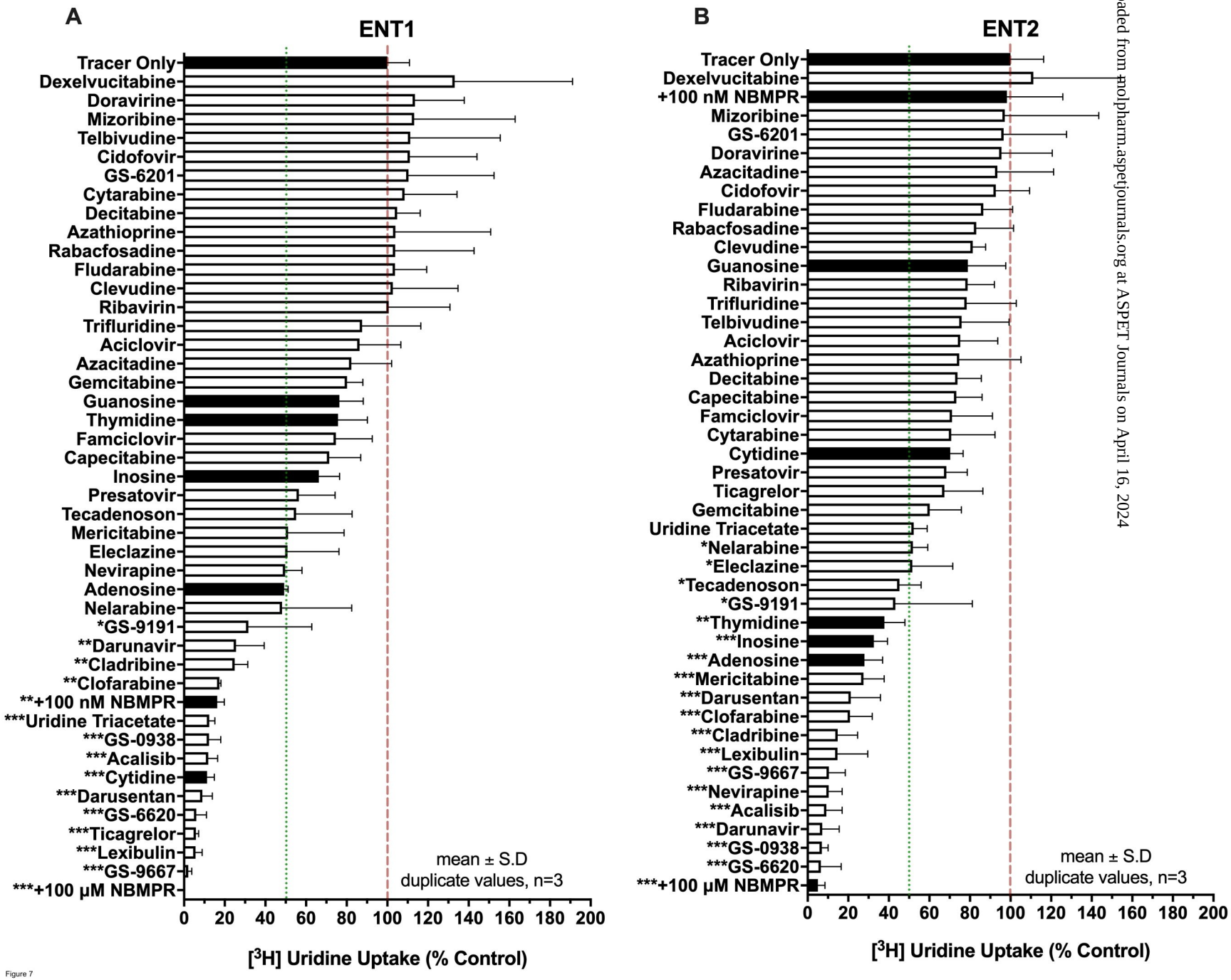

Downloaded from molpharm.aspetjournals.org at ASPET Journals on April 16, 2024

Figure 7

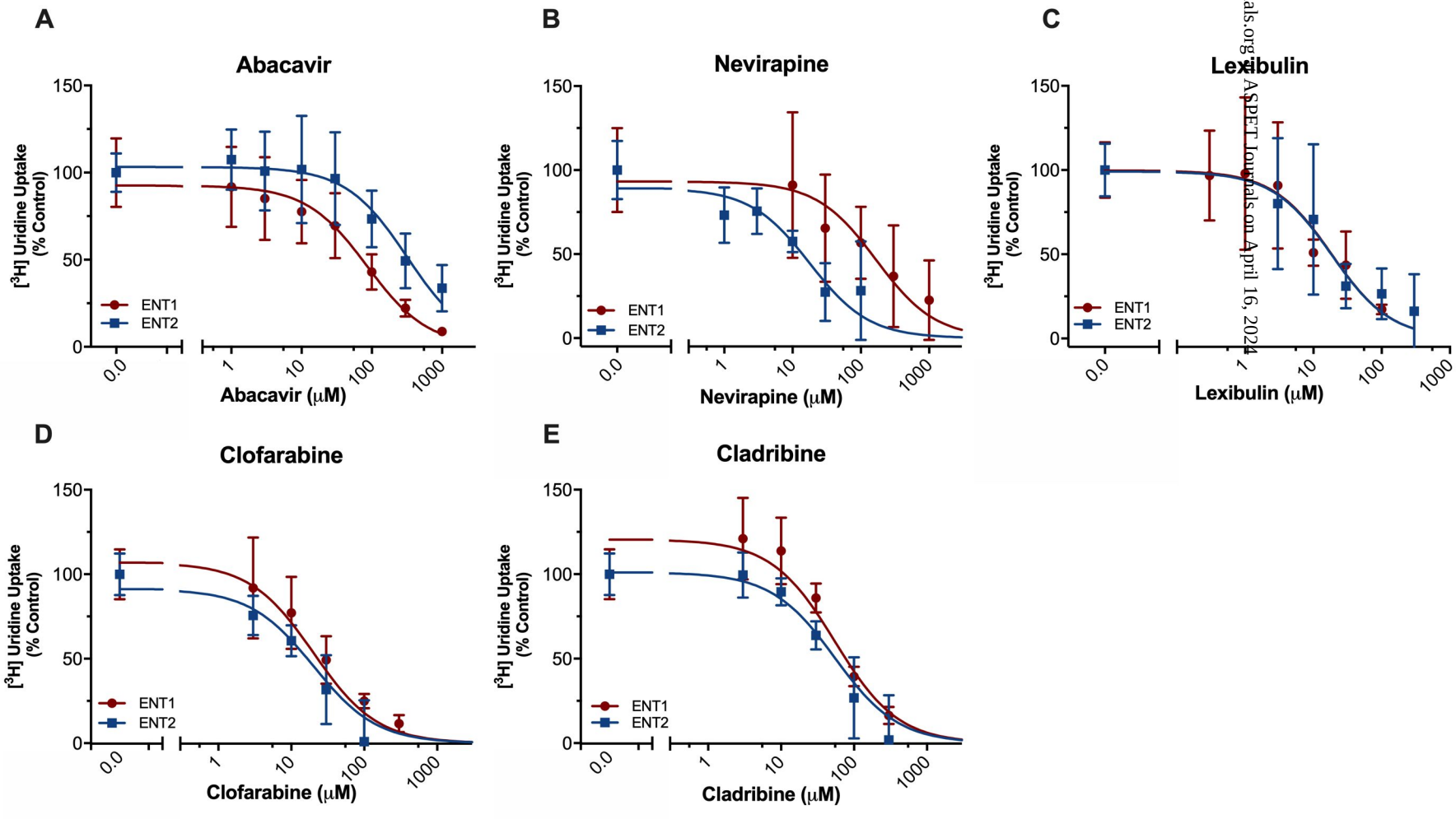

nals.org ASPET Journals on April 16, 2024

Figure 8

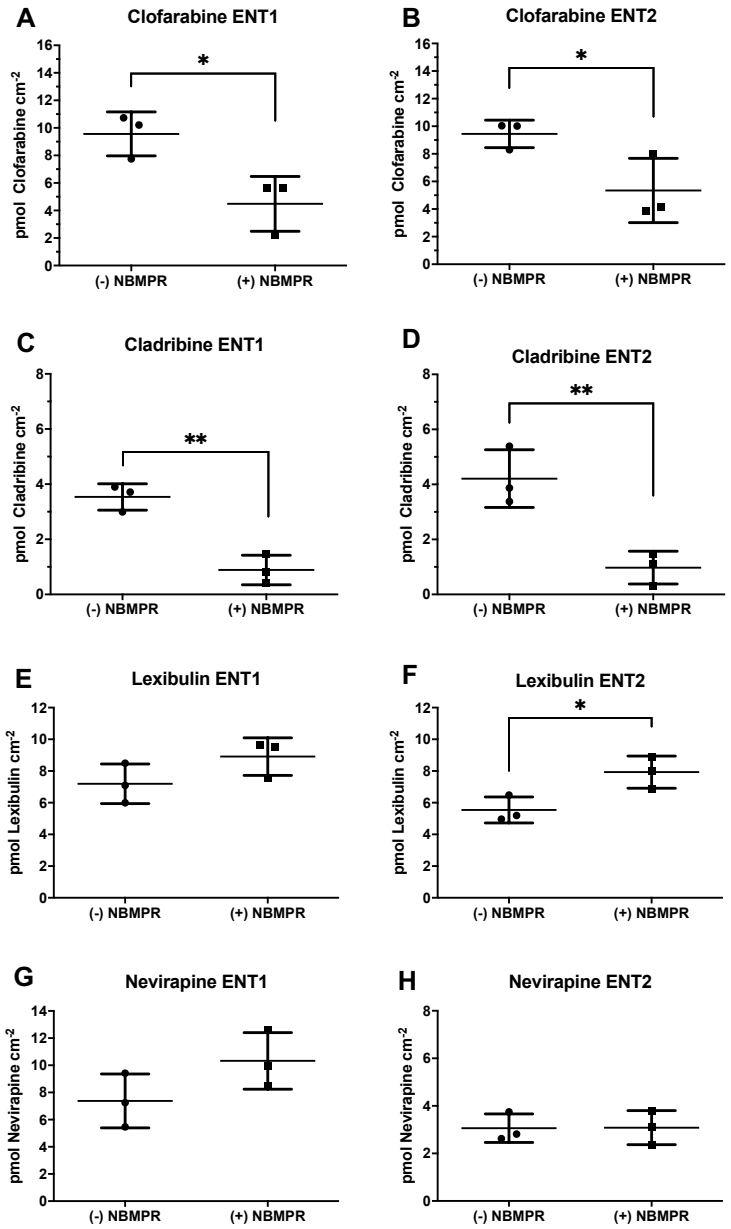

Figure 9

Downloaded from molpharm.aspetjournals.org at ASPET Journals on April 16, 2024

Downloaded from molpharm.aspetjournals.org at ASPET Journals on April 16, 2024

A

ENT1-%uptake

Origin:	Assay Central
Field:	ENT/ent1
Comments:	Threshold: > 0.5
Training Actives:	18 / 44
ROC:	0.7158 (five-fold)
Curve:	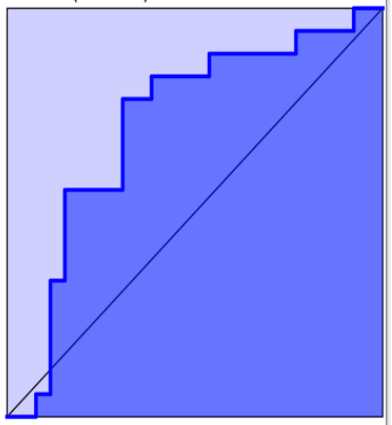

Truth Table:

		Predicted Yes	Predicted No
Actual	**Yes**	14	4
	No	8	18

Precision:	0.6364
Recall:	0.7778
Specificity:	0.6923
F1 score:	0.7000
Kappa:	0.4545
MCC:	0.4623

B

ENT2-%uptake

Origin:	Assay Central
Field:	ENT/ent2
Comments:	Threshold: > 0.5
Training Actives:	17 / 44
ROC:	0.7102 (five-fold)
Curve:	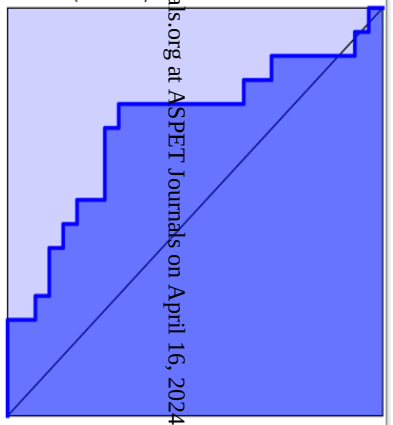

Truth Table:

		Predicted Yes	Predicted No
Actual	**Yes**	13	4
	No	8	19

Precision:	0.6190
Recall:	0.7647
Specificity:	0.7037
F1 score:	0.6842
Kappa:	0.4489
MCC:	0.4566

Figure 10

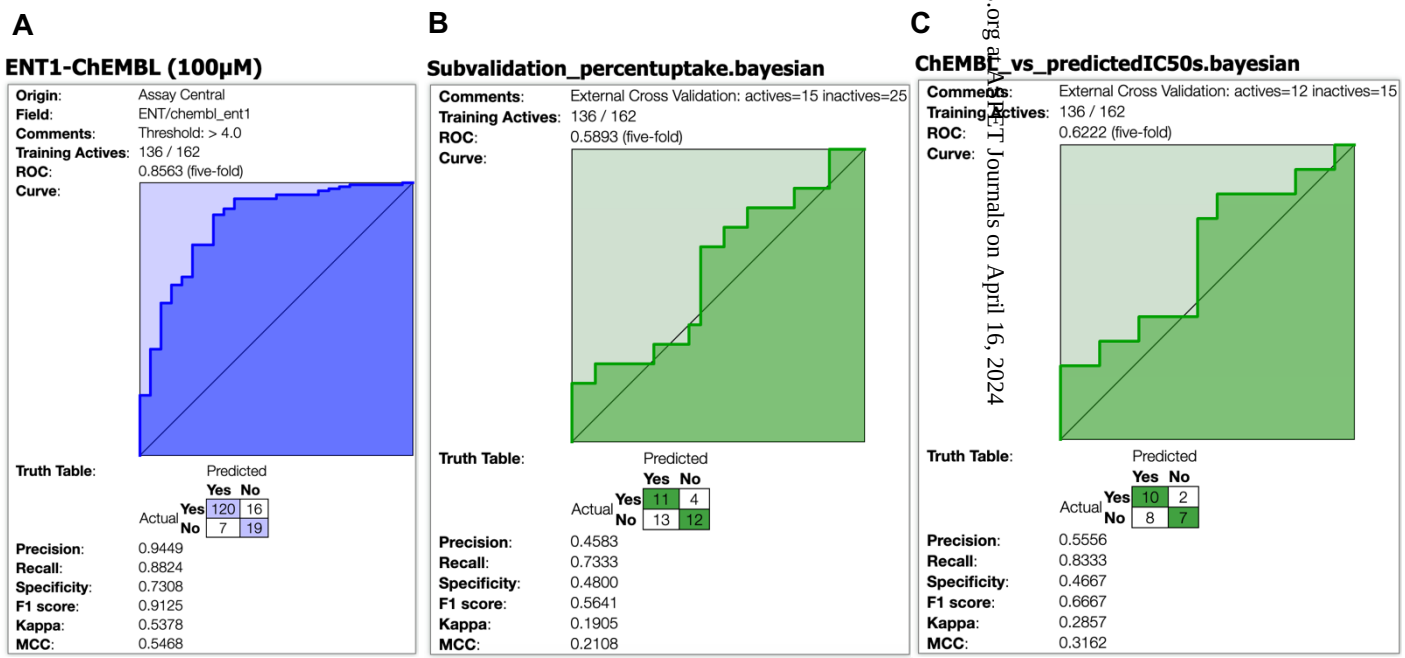

Figure 11

Downloaded from molpharm.aspetjournals.org at ASPET Journals on April 16, 2024

MOLPHARM000169

Predicting Drug Interactions with Human Equilibrative Nucleoside Transporters 1 and 2 Using Functional Knockout Cell Lines and Bayesian Modeling

Siennah R. Miller, Xiaohong Zhang, Raymond K. Hau, Joseph L. Jilek, Erin Q. Jennings, James J. Galligan, Daniel H. Foil, Kimberley M. Zorn, Sean Ekins, Stephen H. Wright & Nathan J. Cherrington

MOLPHARM000169

Supplementary Table 1: Nucleoside Reverse Transcriptase Inhibitors (NRTIs). List of NRTIs with molecular weights and structures are listed for each NRTI.

Structure	Name	MW (g/mol)
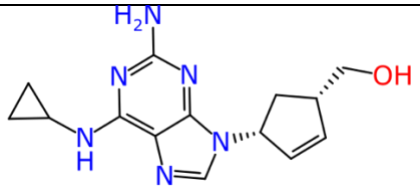	**Abacavir**	**286.33**
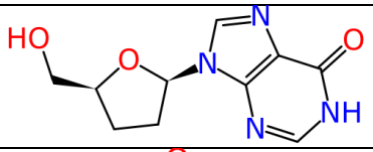	**Didanosine**	**236.23**
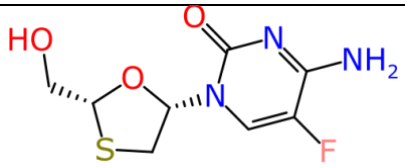	**Emtricitabine**	**247.25**
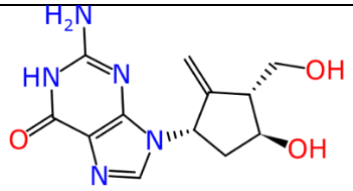	**Entecavir**	**277.28**
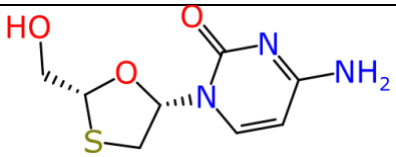	**Lamivudine**	**229.26**
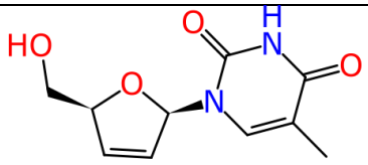	**Stavudine**	**224.21**
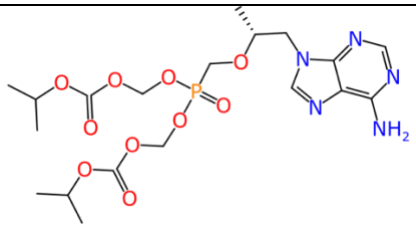	**Tenofovir Disoproxil**	**519.40**
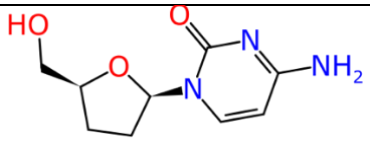	**Zalcitabine**	**211.22**
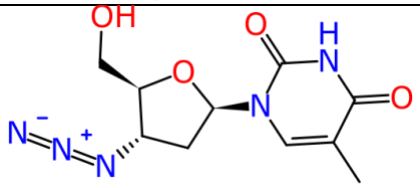	**Zidovudine**	**267.24**

Supplementary Table 2: List of compounds in the library provided by Gilead Sciences. Compounds were provided as 10 mM stocks in DMSO. PubChem Identifiers (CID) and URLs to the 2D structures are listed for each compound.

Analog	CID	PubChem Structure (URL)
Acalisib	11618268	https://pubchem.ncbi.nlm.nih.gov/compound/11618268#section=2D-Structure
Aciclovir	135398513	https://pubchem.ncbi.nlm.nih.gov/compound/135398513#section=2D-Structure
Azacitadine	9444	https://pubchem.ncbi.nlm.nih.gov/compound/9444#section=2D-Structure
Azathioprine	2265	https://pubchem.ncbi.nlm.nih.gov/compound/2265#section=2D-Structure
Capecitabine	60953	https://pubchem.ncbi.nlm.nih.gov/compound/60953#section=2D-Structure
Cidofovir	60613	https://pubchem.ncbi.nlm.nih.gov/compound/60613#section=2D-Structure
Cladribine	20279	https://pubchem.ncbi.nlm.nih.gov/compound/20279#section=2D-Structure
Clevudine	73115	https://pubchem.ncbi.nlm.nih.gov/compound/73115#section=2D-Structure
Clofarabine	119182	https://pubchem.ncbi.nlm.nih.gov/compound/119182#section=2D-Structure
Cytarabine	6253	https://pubchem.ncbi.nlm.nih.gov/compound/6253#section=2D-Structure
Darunavir	213039	https://pubchem.ncbi.nlm.nih.gov/compound/213039#section=2D-Structure
Darusentan	177236	https://pubchem.ncbi.nlm.nih.gov/compound/177236#section=2D-Structure
Decitabine	451668	https://pubchem.ncbi.nlm.nih.gov/compound/451668#section=2D-Structure
Dexelvucitabine	64973	https://pubchem.ncbi.nlm.nih.gov/compound/64973#section=2D-Structure
Doravirine	58460047	https://pubchem.ncbi.nlm.nih.gov/compound/58460047#section=2D-Structure
Eleclazine	71183216	https://pubchem.ncbi.nlm.nih.gov/compound/71183216#section=2D-Structure
Famciclovir	3324	https://pubchem.ncbi.nlm.nih.gov/compound/3324#section=2D-Structure
Fludarabine	657237	https://pubchem.ncbi.nlm.nih.gov/compound/657237#section=2D-Structure
Gemcitabine	60750	https://pubchem.ncbi.nlm.nih.gov/compound/60750#section=2D-Structure
GS-0938/PSI 938	46863668	https://pubchem.ncbi.nlm.nih.gov/compound/46863668#section=2D-Structure

MOLPHARM000169

GS-6201	**11270783**	**https://pubchem.ncbi.nlm.nih.gov/compound/11270783#section=2D-Structure**
GS-6620	**58059494**	**https://pubchem.ncbi.nlm.nih.gov/compound/58059494#section=2D-Structure**
GS-9191	**44181731**	**https://pubchem.ncbi.nlm.nih.gov/compound/44181731#section=2D-Structure**
GS-9667	**11561692**	**https://pubchem.ncbi.nlm.nih.gov/compound/11561692#section=2D-Structure**
Lexibulin	**11351021**	**https://pubchem.ncbi.nlm.nih.gov/compound/11351021#section=2D-Structure**
Mericitabine	**16122663**	**https://pubchem.ncbi.nlm.nih.gov/compound/16122663#section=2D-Structure**
Mizoribine	**104762**	**https://pubchem.ncbi.nlm.nih.gov/compound/104762#section=2D-Structure**
Nelarabine	**3011155**	**https://pubchem.ncbi.nlm.nih.gov/compound/3011155#section=2D-Structure**
Nevirapine	**4463**	**https://pubchem.ncbi.nlm.nih.gov/compound/4463#section=2D-Structure**
Presatovir	**58029842**	**https://pubchem.ncbi.nlm.nih.gov/compound/58029842#section=2D-Structure**
Rabacfosadine	**16047979**	**https://pubchem.ncbi.nlm.nih.gov/compound/16047979#section=2D-Structure**
Ribavirin	**37542**	**https://pubchem.ncbi.nlm.nih.gov/compound/37542#section=2D-Structure**
Tecadenoson	**158795**	**https://pubchem.ncbi.nlm.nih.gov/compound/158795#section=2D-Structure**
Telbivudine	**159269**	**https://pubchem.ncbi.nlm.nih.gov/compound/159269#section=2D-Structure**
Ticagrelor	**9871419**	**https://pubchem.ncbi.nlm.nih.gov/compound/9871419#section=2D-Structure**
Trifluridine	**6256**	**https://pubchem.ncbi.nlm.nih.gov/compound/6256#section=2D-Structure**
Uridine Triacetate	**20058**	**https://pubchem.ncbi.nlm.nih.gov/compound/20058#section=2D-Structure**

Supplementary Table 3: MRM transitions and calibration ranges for compounds used.

Abacavir served as an internal standard (IS) for nevirapine and lexibulin quantification, cladribine served as an IS for clofarabine quantification, and clofarabine served as an IS for cladribine quantification. DP, declustering potential; CE, collision energy. Entrance potential and collision cell exit potentials were both 10 V for all analytes.

Analyte	Parent Ion (Da)	Product Ion (Da)		Range (ng/mL)	R^2	DP (V)	CE (eV)
Clofarabine	**304.1**	**170.1**	**(Quantifier)**	**5-100**	**0.9963**	**50**	**28**
		134.1	**(Qualifier)**			**50**	**55**
Cladribine	**286.0**	**170.0**	**(Quantifier)**	**5-100**	**0.9968**	**30**	**25**
		117.1	**(Qualifier)**			**40**	**25**
Nevirapine	**267.2**	**226.1**	**(Quantifier)**	**5-50**	**0.9914**	**90**	**15**
		230.9	**(Qualifier)**			**80**	**35**
Lexibulin	**435.4**	**257.0**	**(Quantifier)**	**10-100**	**0.9834**	**65**	**33**
		360.2	**(Qualifier)**			**65**	**40**
Abacavir	**287.1**	**150.0**	**(IS)**			**80**	**40**

MOLPHARM000169

Supplemental File 1: Bayesian Modeling Output.

Prediction scores, applicability scores, percent uptake data, predicted and actual IC50 data is included. The green box indicates the compound was predicted to interact with ENT1 based on the Bayesian model generated from the ChEMBL dataset. Red indicates it was not predicted to interact with ENT1, and yellow indicates a potential interaction (close to the 0.5 cutoff for prediction score).

	ENT1 - ChEMBL - Threshold 100μM			Internal data							
Name	Prediction	Applicability		avg%uptake_ENT1	active_ENT1	avg%uptake_ENT2	active_ENT2	edictedIC50_ENT1_u	edictedIC50_ENT2_u	IC50_ENT1_uM	IC50_ENT2_uM
Acalisib	0.5464	0.3659		0.11939	1	0.093528654	1	27.11	20.63		
Aciclovir	0.3941	0.4510		0.863315	0	0.767707663	0	1263	661		
Adenosine	0.2045	In model		0.492505	1	0.286220219	1	194.1	80.2	39.92	56.55
Azacitadine	0.5076	0.7174		0.823231	0	0.955086929	0	931.4	4253		
Azathioprine	-0.4164	0.6545		1.039642	0	0.763361236	0		645.2		
Capecitabine	0.6644	0.6232		0.713873	0	0.748390212	0	499	594.9		
Cidofovir	0.3728	0.3878		1.11094	0	0.947359948	0		3599		
Cladribine	0.6219	0.7895		0.24851	1	0.151481005	1	66.14	35.7		
Clevudine	0.5651	0.4600		1.026723	0	0.830972312	0		1465		
Clofarabine	0.5085	0.6379		0.174278	1	0.212813909	1	42.21	54.07		
Cytarabine	0.3521	0.7174		1.084683	0	0.722311655	0		520.2		
Cytidine	0.3307	0.7174		0.11328	1	0.717482292	0	25.55	507.9	21.08	368.2
Darunavir	0.5480	0.3804		0.255843	1	0.073245332	1	68.76	15.81		
Darusentan	0.6926	0.4706		0.09034	1	0.217160335	1	19.86	55.48		
Decitabine	0.6275	0.7292		1.047812	0	0.754185448	0		613.6		
Dexelvucitabine	0.4944	0.4167		1.330843	0	1.135705087	0				
Doravirine	0.4229	0.4267		1.135591	0	0.975853187	0		8083		
Eleclazine	0.6977	0.4384		0.509334	0	0.526722473	0	207.6	222.6		
Famciclovir	0.4365	0.5172		0.746415	0	0.726175145	0	588.7	530.4		
Fludarabine	0.5040	0.8000		1.037616	0	0.883612363	0		1518		
Gemcitabine	0.3707	0.5000		0.801583	0	0.614133934	0	808	318.3		
GS-0938	0.3740	0.4706		0.122672	1	0.071313587	1	27.96	15.36		
GS-452269	0.4095	0.3976		1.104376	0	0.986477785	0				
GS-465346	0.5221	0.3009		0.059823	1	0.066484224	1	12.72	14.24		
GS-9191	0.3311	0.5361		0.474267	1	0.661622666	0	180.4	391.1		
GS-9667	0.9146	0.8276		0.021066	1	0.107050869	1	4.303	23.98		
Guanosine	0.4775	0.6140		0.763838	0	0.805859627	0	646	830	385.9	254.9
Inosine	0.5877	0.5741		0.66328	0	0.333306504	1	394	99.99	219.5	27.02
Lexibulin	0.7533	0.4368		0.056681	1	0.150032196	1	12.02	35.3		
Mericitabine	0.2985	0.4203		0.511918	0	0.28090792	1	209.8	78.13		
Mizoribine	0.6342	0.7021		1.13182	0	0.991790084	0				
Nelarabine	0.4528	0.8793		0.482309	1	0.52962009	0	186.3	225.2		
Nevirapine	0.5738	0.4259		0.497812	1	0.106084997	1	198.3	23.73		
Presatovir	0.6189	0.3402		0.564572	0	0.698164842	0	259.3	462.6		
Rabacfosadine	0.2729	0.5432		1.038175	0	0.848358017	0		1119		

MOLPHARM000169

Ribavirin	0.6222	0.5870		1.006401	0	0.80537669	0		827.6		
Tecadenoson	0.7321	**In model**		0.551443	0	0.462009015	1	245.9	171.8		
Telbivudine	0.5785	0.4898		1.113105	0	0.774951706	0		688.7		
Thymidine	0.6553	0.7143		0.757414	0	0.386429491	1	624	126	708.9	138.1
Ticagrelor	0.7933	0.3535		0.058287	1	0.688023181	0	12.38	441.1		
Tracer+100uM NBMPR	0.8904	**In model**		-0.007495	1	0.051352222	1			0.01381	1.85
Tracer+5mM Uridine	0.5339	**In model**		-2.61E-18	1	-1.80175E-18	1				
Trifluridine	0.7069	0.7115		0.875326	0	0.800064392	0	1404	800.3		
Uridine Triacetate	0.5028	0.6552		0.124209	1	0.53348358	0	28.36	228.7		

	ENT1 - Miller - Threshold <50%uptake		ENT2 - Miller - Threshold <50%uptake										
Name	**Prediction**	**Applicability**	**Prediction**	**Applicability**		**avg%uptake_ENT1**	**active_ENT1**	**avg%uptake_ENT2**	**active_ENT2**	**edictedIC50_ENT1_u**	**edictedIC50_ENT2_u**	**IC50_ENT1_uM**	**IC50_ENT2_uM**
Adenosine	0.5463	0.8679	1.2555	0.8679		0.492505	1	0.286220219	1	194.1	80.2	39.92	56.55
Cytidine	-1.0099	0.9783	-0.4131	0.9783		0.11328	1	0.717482292	0	25.55	507.9	21.08	368.2
Guanosine	-0.4379	0.8421	-0.5179	0.8421		0.763838	0	0.805859627	0	646	830	385.9	254.9
Inosine	-0.0598	0.7222	-0.0156	0.7222		0.66328	0	0.333306504	1	394	99.99	219.5	27.02
Thymidine	-0.4465	0.9592	-0.8471	0.9592		0.757414	0	0.386429491	1	624	126	708.9	138.1